

PREPRINT SUBMITTED: This manuscript is a preprint uploaded to EarthArXiv, not yet peer-reviewed. This preprint is submitted for publication to Quaternary Science Reviews in February 2024. Authors encourage downloading the latest manuscript version from EarthArXiv, and welcome comments, feedback and discussions. Please, feel free to get in contact with the first author: denovan.chauveau@unive.it

Sea-level oscillations within the Last Interglacial: insights from coral reef stratigraphic forward modelling

Denovan Chauveau^{a*}, Nikos Georgiou^a, Ciro Cerrone^a, Silas Dean^a, Alessio Rovere^{a,b}

^aDepartment of Environmental Sciences, Informatics and Statistics, Ca' Foscari University of Venice, Italy

^bMARUM, Center for Marine Environmental Sciences, University of Bremen, Germany

**Corresponding author: denovan.chauveau@unive.it*

1 **Sea-level oscillations within the Last Interglacial:**
2 **insights from coral reef stratigraphic forward**
3 **modelling**

4
5 Denovan Chauveau^a, Nikos Georgiou^a, Ciro Cerrone^a, Silas Dean^a, Alessio
6 Rovere^{a,b}

7
8 *^aDepartment of Environmental Sciences, Informatics and Statistics, Ca'*
9 *Foscari University of Venice, Italy*

10 *^bMARUM, Center for Marine Environmental Sciences, University of Bremen,*
11 *Germany*

12
13 **Keywords**

14 Marine Isotope Stage 5e; Last Interglacial; Sea level; Fossil coral reef;
15 Stratigraphic forward modelling

16
17 **Abbreviations**

18 Marine Isotope Stage (MIS); Greenland Ice Sheet (GrIS); Antarctic Ice
19 Sheet (AIS); Global Mean Sea Level (GMSL); Relative Sea Level (RSL);
20 Coral Reef Terrace (CRT)

21
22 **Abstract**

24 Understanding past sea-level variations is essential to constrain future
25 patterns of sea-level rise in response to warmer climate conditions. Due to
26 good preservation and the possibility to use various geochemical methods
27 to date fossil sea-level index points, the Last Interglacial (Marine Isotope
28 Stage, MIS, 5e, 130-116 ka) is often regarded as one of the best climate
29 analogs for a future warmer climate. MIS 5e coastal stratigraphic
30 sequences, such as fossil coral reefs in tectonically stable areas, are
31 characterized by abrupt shifts in their geological facies, steps within the reef
32 topography or backstepped fossil reefs, which have been often interpreted
33 as proxies for abrupt sea-level fluctuations within the interglacial. However,
34 the observational evidence and magnitude of such abrupt changes are
35 controversial. Here, we run nearly 50 thousand simulations of a 2D
36 kinematic reef model that can reproduce coral reef growth and demise
37 through time. Our aim is to investigate the parameters of space, the sea-
38 level scenarios, and the processes which multiple-stepped MIS 5e fossil
39 reefs form. As inputs to the model, we use both published and synthetic
40 sea-level histories (17 sea-level curves ranging from one to several sea-
41 level peaks), and a wide range of reef growth rates, marine erosion rates
42 and bedrock foundation slopes. Our results show that the only sea-level
43 history that could explain the generation of an emerged MIS 5e backstepped
44 reef is a first sea-level peak followed by an abrupt rise in sea level and a
45 second short-term peak. Any other multiple-stepped stratigraphy can be
46 explained by the interplay between reef growth, marine erosion, and
47 bedrock slope.

48

49 **1. Introduction**

50

51 In less than a century, global atmospheric temperatures will likely be 2°C
52 higher than in the pre-industrial period (Raftery et al., 2017), leading to a
53 sea-level rise up to 1 m by 2100 (high-end SSP5-8.5 scenario from the AR6
54 Intergovernmental Panel on Climate Change, IPCC; Fox-Kemper et al.,
55 2021). In this context, it is crucial to constrain future fluctuations in sea
56 level to rapidly draw up adaptation plans. Substantial uncertainties
57 regarding future sea-level scenarios are related to the response of the
58 Greenland and Antarctic Ice Sheets (GrIS and AIS) to global warming
59 (Horton et al., 2020). DeConto et al. (2021) show that melting pulses
60 caused by AIS retreat could lead to sea-level rise rates an order of
61 magnitude higher than today. To accurately assess the current instability of
62 ice sheets, it is crucial to enhance our understanding of past meltwater
63 pulses during fast sea-level transgressions (Liu et al., 2015) and
64 interglacials (Deiana et al., 2021).

65

66 The Last Interglacial (Marine Isotope Stage, MIS, 5e, 130-116 ka ago) was
67 the last period of the Earth's history when the climate was warmer than
68 pre-industrial. As a result, MIS 5e ice sheets were smaller than today, and
69 global mean sea level (GMSL) was 2-9 m above present mean sea level
70 (e.g., Dutton & Lambeck, 2012; Dyer et al., 2021; Dumitru et al., 2023).
71 The existence and possible patterns of abrupt GMSL changes within MIS 5e

72 are still debated (Dutton & Barlow, 2019). Indeed, several coastal features
73 associated with MIS 5e are characterized by abrupt shifts in geological facies
74 (see Section 2), that many authors attributed to rapid relative sea-level
75 (RSL) changes or fluctuations within the interglacial (Hearty et al., 2007;
76 O’Leary et al., 2013; Vyverberg et al., 2018). One critical point is that these
77 proxies, mainly from coral reef areas, are subject to several uncertainties,
78 stemming from the dating and interpretation of paleowater depth of fossil
79 corals (Hibbert et al., 2016; Polyak et al., 2018). This limits our ability to
80 draw conclusions about possible MIS 5e GMSL fluctuations (Dutton &
81 Barlow, 2019).

82

83 Multi-meter GMSL fluctuations (e.g., low-to-high swings of more than 4 m,
84 Thompson et al., 2005; Kopp et al., 2009) would entail ice regrowth during
85 the Last Interglacial, which is considered highly unlikely as there are no
86 plausible processes that could explain it (Barlow et al., 2018). Non-eustatic
87 processes have been invoked to explain MIS 5e coastal stratigraphies
88 showing signs of possible intra-interglacial sea-level fluctuations, including
89 local tectonic movements (Whitney & Hengesh, 2015) or the effect of
90 topographical variations of antecedent foundations on new reef
91 constructions (Chauveau et al., 2023). Another plausible explanation is that
92 AIS and GrIS evolved asynchronously during MIS 5e and then contributed
93 to GMSL at different times. This would result in an early sea-level highstand
94 (before 125 ka) stemming from AIS melting, followed by a later and more
95 diffuse contribution from GrIS (Rohling et al., 2019; Barnett et al., 2023).

96

97 In this study, we use a numerical model (REEF, Husson et al., 2018; Pastier
98 et al., 2019) that simulates the growth and erosion of coral reefs through
99 time to investigate the effects of different sea-level histories on their
100 formation during the Last Interglacial. As inputs to the model, we use both
101 published and synthetic sea-level histories, and a wide range of input
102 parameters (i.e., reef growth rate, marine erosion rate and bedrock
103 foundation slope). We ran a total of nearly 50 thousand numerical
104 simulations. We discuss which MIS 5e GMSL conditions are most favorable
105 for the development of stratigraphic and morphological characteristics that
106 may be interpreted as evidence for sea-level fluctuations during the
107 interglacial.

108

109 **2. Background: Fossil coral reefs**

110

111 Living and fossil corals are widespread around the world's tropical and
112 subtropical areas (Veron et al., 2015; Chutcharavan & Dutton, 2021). Coral
113 reef genesis is strongly influenced by the accommodation space, which
114 corresponds to the interplay between sea-level changes and reef growth,
115 as well as the slope of bedrocks and their availability for coral settlement
116 (Camoin & Webster, 2015). When the sea level falls too rapidly, coral reefs
117 may emerge and die, creating coral reef terraces (CRTs, Murray-Wallace &
118 Woodroffe, 2014). CRTs are expanses of reefal limestone (i.e., the fossil
119 coral-built surfaces) with flat or slightly sloping surfaces, limited seaward

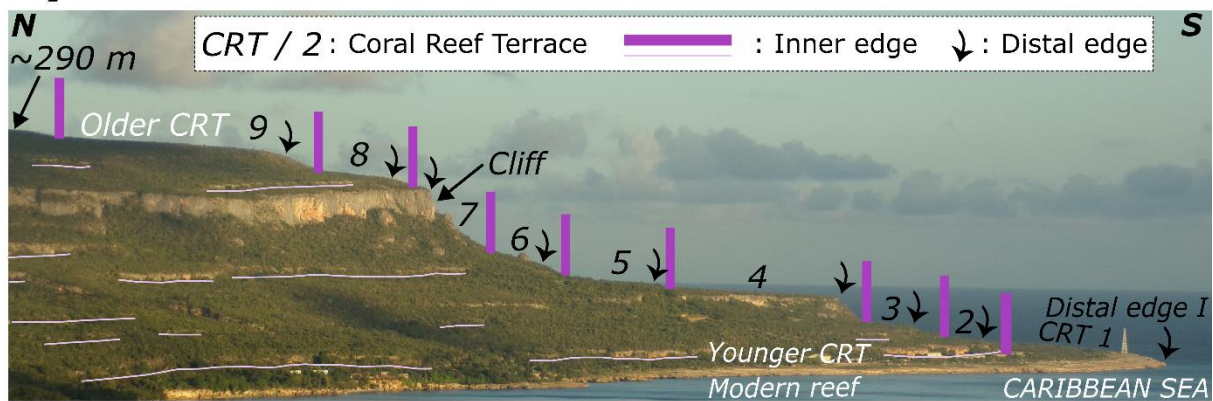
120 by a distal edge over a cliff of variable thickness (e.g., Chappell, 1974; Fig.
121 1A). Landward, CRTs are limited by an inner edge, characterized by a break
122 in slope (Fig. 1).

123

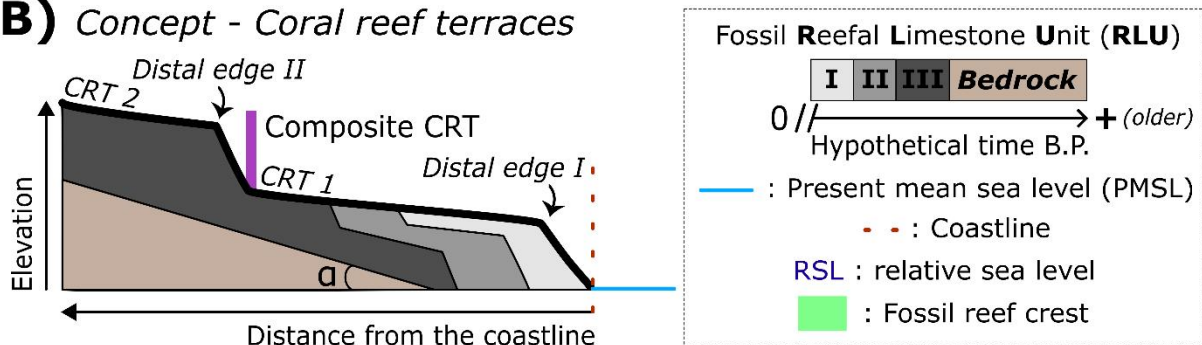
124 The morphology and stratigraphy of CRTs are the result of the interactions
125 between reef accretion (bioconstruction and sedimentation), RSL changes,
126 erosion (marine and continental) and the basement geometry (Camoin &
127 Webster, 2015; Pastier et al., 2019; Chauveau et al., 2021), resulting in a
128 wide spectrum of morphologies (Pedoja et al., 2018). Complex stratigraphic
129 contexts associated with reefs formed during a single highstand have been
130 described both in tectonically stable (e.g., Chen et al., 1991) and uplifting
131 areas (Pedoja et al., 2014). For example, there may be several
132 morphologically distinct CRTs (Fig. 1B, 1C; e.g., de Gelder et al., 2022);
133 reefal limestone units of slightly different ages within a single CRT (Fig. 1B;
134 Chauveau et al., 2021) or separated by an erosional surface or layer of coral
135 rubble (e.g., Thompson et al., 2011); changes in reef facies (e.g.,
136 Bruggemann et al., 2004); or the backstepping of the reef crest (Fig. 1C;
137 e.g., Blanchon, 2010). All these features have been described at several
138 locations globally (see the compilation in Hearty et al., 2007, Rohling et al.,
139 2019, and Dutton et al., 2022), but their origin is still controversial.

140

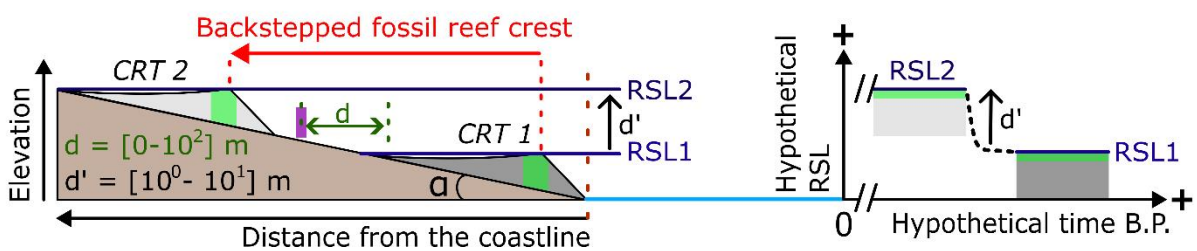
A) Example of coral reef terrace sequence (Punta Caleta, SE Cuba)



B) Concept - Coral reef terraces



C) Concept - Backstepped fossil coral reef



141 **Figure 1. A)** View from the west of Punta Caleta (south-east Cuba). The
 142 coral reef terrace sequence visible in the image is around 1.5 kilometers
 143 long. The inner edges drawn on the image are only those visible and
 144 therefore do not represent all of those mapped by Peñalver et al. (2021).
 145 The highest terrace in this area is estimated to be several million years old.
 146 The tectonic uplift rate affecting the area has been calculated at 0.23 ± 0.07
 147 mm a^{-1} (Authemayou et al., 2023). The cliff shown in the image is the
 148 highest in the sequence. Schematic concept of **B)** a CRT including several
 149 reefal limestone units and **C)** a backstepped fossil coral reef. The process

150 *of backstepping consists of the abrupt demise of a reef (CRT 1) and the*
151 *construction of a new reef surface (CRT 2), topographically higher than the*
152 *previous one (Blanchon, 2010; Camoin & Webster, 2015). The cause of reef*
153 *backstepping is a rapid rise in RSL (elevation d' , i.e., the difference between*
154 *RSL1 and RSL2), which drowns the older reef and prevents coral growth*
155 *due to the RSL rising faster than the reef growth rate. CRTs 1 and 2 may*
156 *be separated by relatively long distance (d ; e.g., Blanchon, 2010).*

157

158 **3. Methodology: Fossil coral reef modeling**

159

160 Coastal landscape evolution models can be used to assess the geometry of
161 a marine terrace sequence, to constrain the chrono-stratigraphy, and to
162 unravel the influence of processes involved in their morphogenesis (de
163 Gelder et al., 2020; Georgiou et al., 2022; Matsumoto et al., 2022; Boyden
164 et al., 2023). Since the pioneering work of Chappell (1980), several
165 numerical models of reef growth have been developed (Turcotte & Bernthal,
166 1984; Bosscher & Schlager, 1992; Webster et al., 2007; Koelling et al.,
167 2009; Toomey et al., 2013). Here, we use the kinematic Fortran code model
168 REEF, developed by Husson et al. (2018) and Pastier et al. (2019). REEF is
169 a profile evolution model that considers past eustatic sea-level oscillations,
170 vertical land motion, reef growth, marine erosion, and the resulting
171 deposition of the eroded clastic sediments, modelling on an initially linear
172 slope.

173

174 Reef growth in REEF is defined through a potential reef growth rate,
175 consisting of a vertical component of aggradation (accounting for the
176 decreasing coral growth rate with increasing depth as a response to light
177 attenuation) and a horizontal component of progradation (considering the
178 decreasing coral growth from the reef crest, facing the open sea, towards
179 the shore). Marine erosion is based on the wave erosion model of Anderson
180 et al. (1999). It integrates a vertical seabed erosion component as well as
181 a horizontal cliff erosion component. In the REEF model, these are
182 approximated by an eroded volume, in which the proportions between
183 vertical and horizontal erosions rely on wave dissipation (Anderson et al.,
184 1999). Clastic sediment deposition reflects the eroded rock volume, in which
185 horizontal deposition occurs in reef flats or inner lagoons if any (i.e., several
186 meters deep, e.g., Kennedy et al., 2021), and at a repose angle of 10% at
187 the base of the forereef slope. The temporal and spatial resolution are
188 respectively 1 ka and 1 m. We refer the reader to Husson et al. (2018),
189 Pastier et al. (2019), and Chauveau et al. (2023) for more details about
190 REEF code.

191
192 Our approach aims to constrain the parametric conditions with which the
193 REEF model can recreate multiple CRTs associated with MIS 5e, and ideally
194 to recreate a younger unit on top of an older one, in a hypothetical case of
195 a tectonically stable area. For this purpose, we free the model from tectonics
196 as input and use a wide range of values for each parameter (Table 1). These
197 ranges have been chosen on the basis of previous studies (maximum reef

198 growth rate, Dullo, 2005; bedrock slope, Chen et al., 1991, Rovere et al.,
199 2018), to study extreme cases (maximum reef growth rate of 50 mm a⁻¹)
200 or because very few constraints exist (erosion rate; see Section 5.2.). To
201 simulate reef growth and demise under different sea-level scenarios we use
202 different GMSL curves from the following sources: Waelbroeck et al. (2002),
203 Bintanja et al. (2005), Kopp et al. (2009), Rohling et al. (2009), Spratt &
204 Lisiecki (2016), Rohling et al. (2019), and Dumitru et al. (2023) (Fig. 2A,
205 see the description of these curves in the supplementary information,
206 Section SI.1.). In addition to these proxy-based GMSL curves, we also
207 created synthetic sea-level scenarios that reproduce intra-interglacial
208 fluctuations (Fig. 2B, 2C, 2D). These synthetic curves have a duration of 15
209 ka. The maximum and the minimum ages are set because they correspond
210 to the most widely accepted age limits: 130 ka (Rohling et al., 2019) and
211 116 ka (Rovere et al., 2016; Dutton & Barlow, 2019), respectively. This
212 time step also makes it possible to create sea-level curves with an axis of
213 symmetry at 123 ka (Fig. 2B, 2C, 2D). These synthetic curves have a
214 maximum amplitude variability of 18 m (i.e., between -9 and 9 m relative
215 to present sea level) to consider the maximum sea-level value at MIS 5e
216 (e.g., Kopp et al., 2009, 2013; Dutton & Lambeck, 2012). In total, we ran
217 49980 simulations (2940 per each single sea-level scenario) using
218 permutations of the parameters shown in Table 1. To gauge the ability of
219 each simulation to reproduce a scenario of multiple fossil CRTs, we adopt a
220 score based on 3 criteria, as shown in Table 2.

Symbol	Definition	Permuted value(s)	Unit
α	Initial bedrock slope	1, 2, 3, 4, 5, 6, 8, 10, 15, 20, 25, 30, 40, 50	%
G_{\max}	Maximum reef growth rate	1, 2, 3, 4, 5, 6, 8, 10, 15, 20, 25, 30, 40, 50	mm a ⁻¹
E	Erosion rate	1, 5, 10, 20, 30, 40, 50, 60, 80, 100, 150, 200, 300, 400, 500	mm ³ a ⁻¹
Z_{\max}	Maximum reef growth depth	20	m
Z_{\min}	Optimal reef growth depth	2	m
Z_0	Maximum depth of wave erosion	3	m

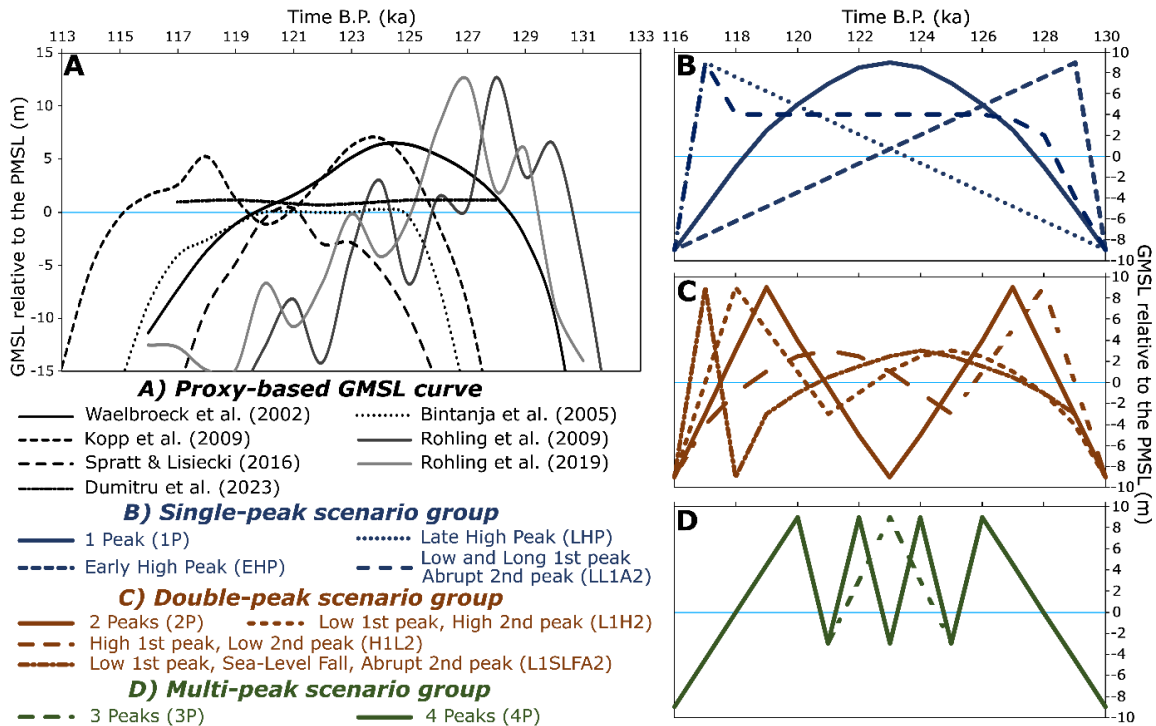
221 **Table 1.** Model input parameters, symbols, values, and units. The minimum possible value as model input for all
222 parameters is 1. The maximum and optimal reef growth depths (Z_{\max} and Z_{\min} , respectively) and the maximum depth
223 of wave erosion (Z_0) are based on previous studies: 20 m, 2 m (Bosscher & Schlager, 1992) and 3 m (Pastier et al.,
224 2019), respectively.

225

Criterion	Definition	Total point
0	Submerged CRT	0
I	One emerged CRT or reefal limestone unit	1
II	Multiple emerged CRTs	2
III	The youngest CRT is above the oldest CRT	3

226 **Table 2.** Criteria for scoring simulations. When the reef reproduced by a simulation fills a criterion, the simulation
227 is scored with 1 point. The maximum score attainable is 3 points.

228

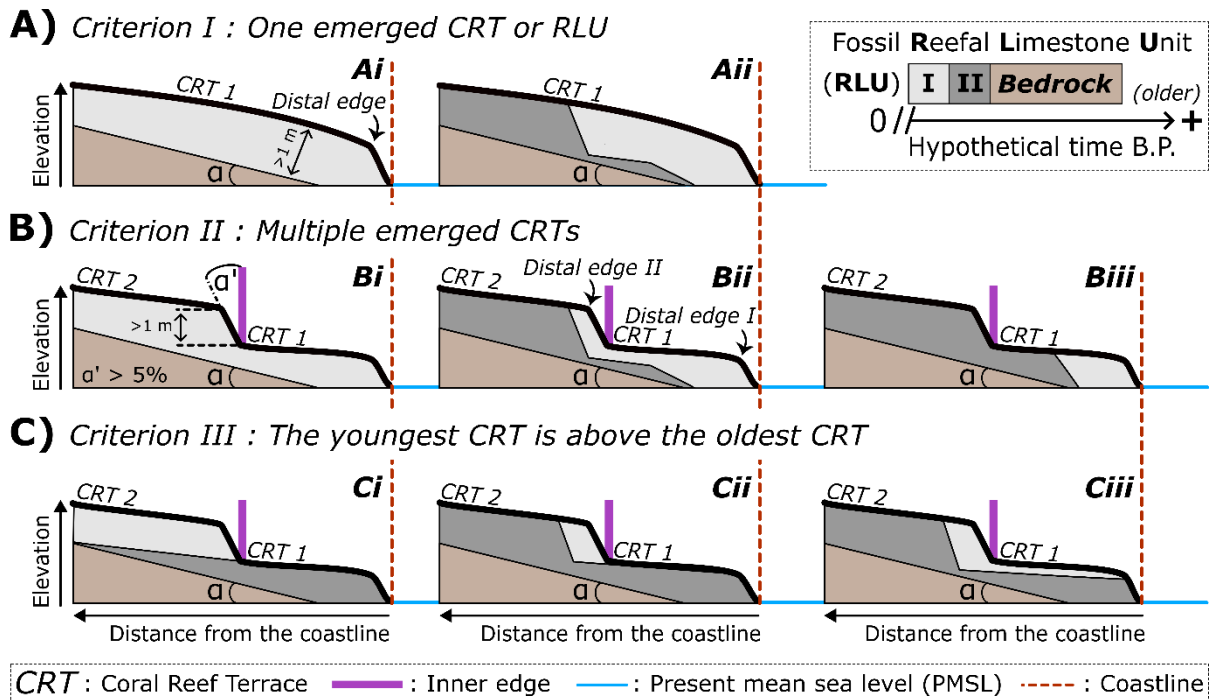


229 **Figure 2.** Sea-level scenarios for the MIS 5e used in this study as inputs in
 230 the model of Pastier et al. (2019): **A)** proxy-based GMSL curves, and
 231 synthetic sea-level curves divided in three groups: **B)** Single-peak, **C)**
 232 Double-peak, **D)** Multi-peak GMSL scenarios. The sea-level curves are
 233 relative to the present mean sea level (PMSL). The sea-level curves of Kopp
 234 et al. (2009) and Dumitru et al. (2023) are the 50th percentile predictions
 235 provided by these authors. The sea-level curve of Rohling et al. (2019) is
 236 the same as that shown in Figure 3a of this article (i.e., GMSL approximation
 237 based on the probabilistically assessed KL11 Probability maximum, PM; see
 238 Section SI.1). The single-peak group includes 1) one major peak (1P); 2) a
 239 relatively stable sea level with a late peak (LHP), or 3) an early peak (EHP);
 240 4) a first flat, relatively long and low peak, followed by a second relatively
 241 high and short peak, separated by an abrupt rise in sea level (LL1A2); The
 242 double-peak group includes 5) two peaks separated by high sea-level fall
 243 (2P); 6) a first relatively low and long peak followed by a sea-level drop and

244 *a second higher and shorter peak (L1H2); 7) a first relatively high and short*
245 *peak followed by a lower and longer peak (H1L2); 8) a first relatively low*
246 *and long peak followed by a second shorter and higher peak, both separated*
247 *by an abrupt sea-level drop (L1SLFA2); and the multi-peak group includes*
248 *9) 3 and 10) 4 peaks. In this study, we consider the length of a sea-level*
249 *peak to be the time between the start of the transgression and the end of*
250 *the regression surrounding the sea-level maximum.*

251

252 As the model does not simulate reef facies, we consider a reefal limestone
253 unit to be a unit constructed over 1 ka (i.e., the model time step). A
254 CRT/reefal limestone unit is considered emerged when it is higher than 1 m
255 above present sea level (i.e., corresponding to the uncertainty of the model,
256 Fig. 3A). We consider that the model output has two CRTs when they are
257 separated by a significant slope (i.e., greater than 5%), associated with a
258 cliff of more than 1-m high, overhanging the inner edge (Fig. 3B, 3C). Given
259 the very wide parametric range and the time step of 1 ka, sometimes, the
260 simulations produce morphologies that are not realistic, i.e., morphological
261 surface with concavities of over 1 m. This is primarily because of the 1 ka
262 time step, coupled with excessively high reef growth and insufficient erosion
263 rates. When such emerged irregularities are more than 1 m thick, we
264 consider only criterion I to be valid in order to select only the most realistic
265 simulations.



267 **Figure 3.** Schematic example of different chrono-morphology scenarios
 268 that validate criteria **A) I:** One emerged CRT or reefal limestone unit, **B) II:**
 269 Multiple emerged CRTs, **C) III:** The youngest CRT is above the oldest CRT.
 270 Elevations and distances not to scale. Criterion III is valid even if the
 271 terraces contain several reefal limestone units, as in Cii-iii.

272

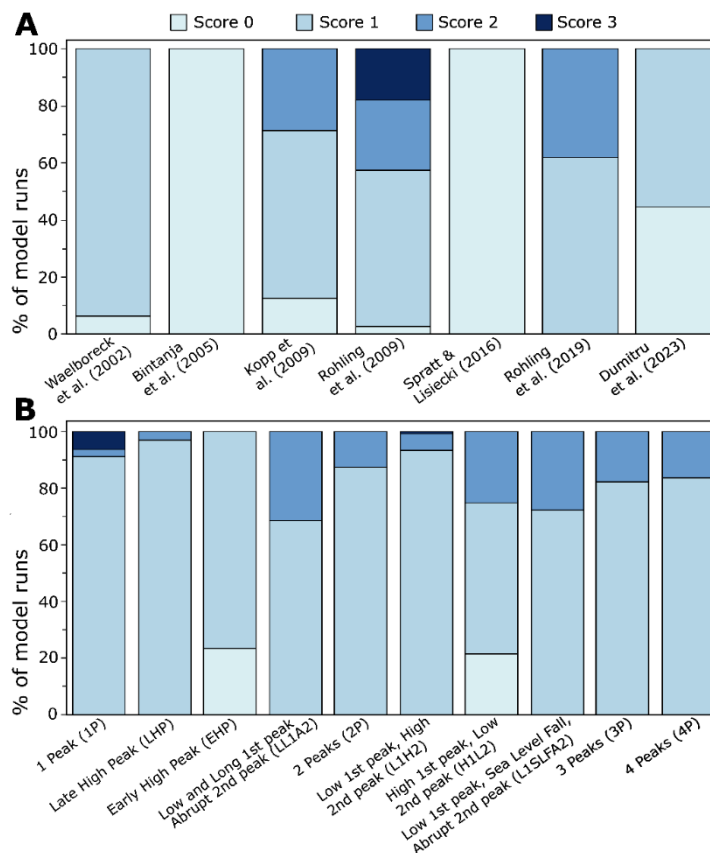
273 **4. Results**

274

275 Of the 49980 simulations, 2 proxy-based GMSL curves (i.e., from Bintanja
 276 et al., 2005 and Spratt & Lisiecki, 2016), representing 12% of our
 277 simulations (5880 simulations), were discarded from further analysis, as
 278 they scored zero (Fig. 4). Out of the remaining 44100 simulations, 7%
 279 reached a score of zero (3252 simulations), 75% a score of 1 (33242
 280 simulations), 16% a score of 2 (6875 simulations) and 2% (731

281 simulations) reached a score of 3 (Fig. 4). In the supplementary information
 282 (Section SI.2.), we describe all the results as well as parametric trends for
 283 the proxy-based GMSL (Fig. SI1) and synthetic sea-level curves (Figs. SI2;
 284 SI3; SI4) scenarios. Below, we describe the set of morphologies obtained
 285 by simulations reaching scores of 3 and 2, and then discuss the relationship
 286 between marine erosion rate and initial bedrock slope.

287



288 **Figure 4.** Percentage of scores for the **A)** proxy-based and **B)** synthetic
 289 sea-level curves.

290

291 **4.1. The youngest CRT is above the oldest CRT (Score of 3)**

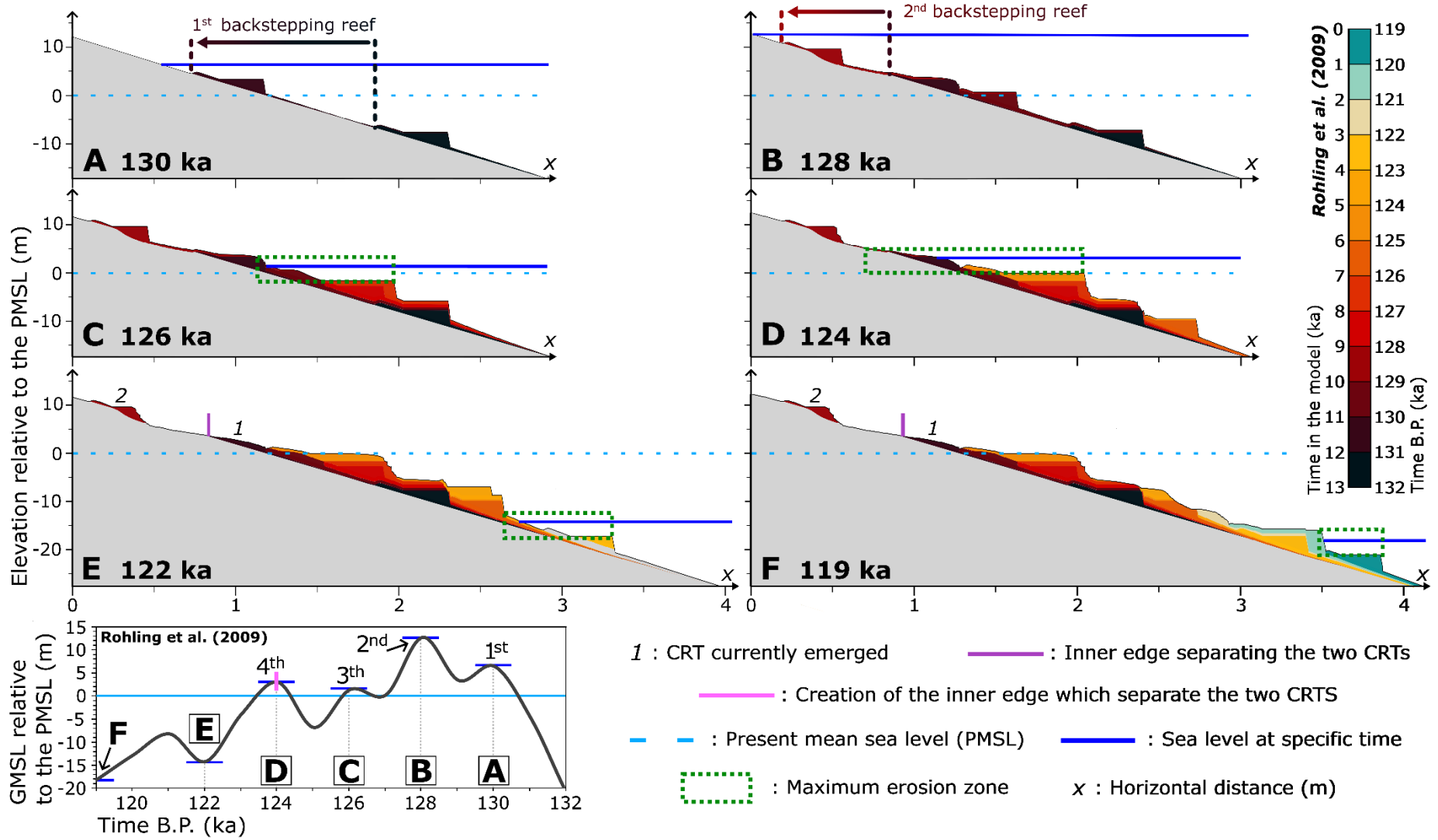
292

293 On the 44100 simulations, 731 reached a score of 3. Among these, 72%
 294 have as input the multi-peak GMSL curve of Rohling et al. (2009) (523

295 simulations). The other high scores are attained by synthetic sea-level
296 curves, 25% of those with one major peak (i.e., 1P, 183 simulations) and
297 3% among the Low 1st peak, High 2nd peak (i.e., L1H2, 25 simulations)
298 scenarios.

299

300 Some simulations from the GMSL curve of Rohling et al. (2009) show the
301 abrupt demise of CRTs (Fig. 5A, 5B). In these cases (Fig. SI1), a reef is first
302 demised (at 131 ka) and another reef is built higher up (from 131 to 130
303 ka ago, Fig. 5B). This new reef is then demised (at 129 ka), to make way
304 for a new 129/128 ka reef built during the sea-level maximum of this
305 scenario (2nd peak), around 7 m higher up and at around 400 m landward
306 (Fig. 5B). During this period, a reef veneer reoccupies the 131/130 ka fossil
307 reef (Fig. 5B). This thin coral layer is then eroded during the subsequent
308 sea-level oscillations (Fig. 5C, 5D). Finally, the two CRTs (1 and 2, Fig. 5E,
309 5F) emerge during the following sea-level regression. The simulations, that
310 successfully reproduce the backstepping process (Fig. SI1), are all in the
311 range of α (initial bedrock slope) = [1-15] % and E (erosion rate) = [20-
312 500] $\text{mm}^3 \text{a}^{-1}$ and are only valid for G_{max} (maximum reef growth rate) = 1
313 mm a^{-1} (Fig. SI1).



315 **Figure 5.** Formation of coral reef terraces with the GMSL curve of Rohling
316 et al. (2009) at different steps: **A)** 130, **B)** 128, **C)** 126, **D)** 124, **E)** 122,
317 **F)** 119 ka ago. These steps are placed by the dark blue line on the sea-level
318 curve at the bottom left. The parameters of the selected simulation are as
319 follows: a (initial bedrock slope) = 1%, G_{max} (maximum reef growth rate)
320 = 1 mm a⁻¹, E (erosion rate) = 400 mm³ a⁻¹. The maximum erosion zone is
321 5 m relative to the sea level at the specific time (3 m below and 2 m above).
322 The 5 m value corresponds to the maximum depth of wave erosion (i.e., 3
323 m; Table 1), plus cliff erosion (i.e., 1 m, Pastier et al., 2019), plus model
324 uncertainty (i.e., 1 m). As the model does not simulate reef facies such as
325 the reef crest, we take the inner edges as the reference for the backstepping
326 process.

327
328 The simulations with score 3 from the one major peak scenario (1P) all show
329 the same morphological characteristics: a large, high emerged CRT (around
330 7 m above the present mean sea level) with age of 126/125 ka (Fig. 6B).
331 Below this, a second, less wide CRT of an older age is formed (i.e., 127/126
332 ka; Fig. 6B) emerging around 3 m above the present mean sea level. This
333 type of double CRT is also found with the GMSL curve of Rohling et al.
334 (2009) for G_{max} values > 5/6 mm a⁻¹.

335
336 The simulations that reach the score of 3 with the L1H2 scenario (i.e., a
337 first relatively low and long peak followed by a sea-level drop and a second
338 higher and shorter peak) all show two CRTs emerged around 3 m and 6 m

339 above the present mean sea level (Fig. 6C). The lowest contains two reefal
340 limestone units of ages 120/119 ka and 119/118 ka. The highest CRT is
341 made up of the youngest reefal limestone unit (i.e., age of 119/118 ka; Fig.
342 6C).

343

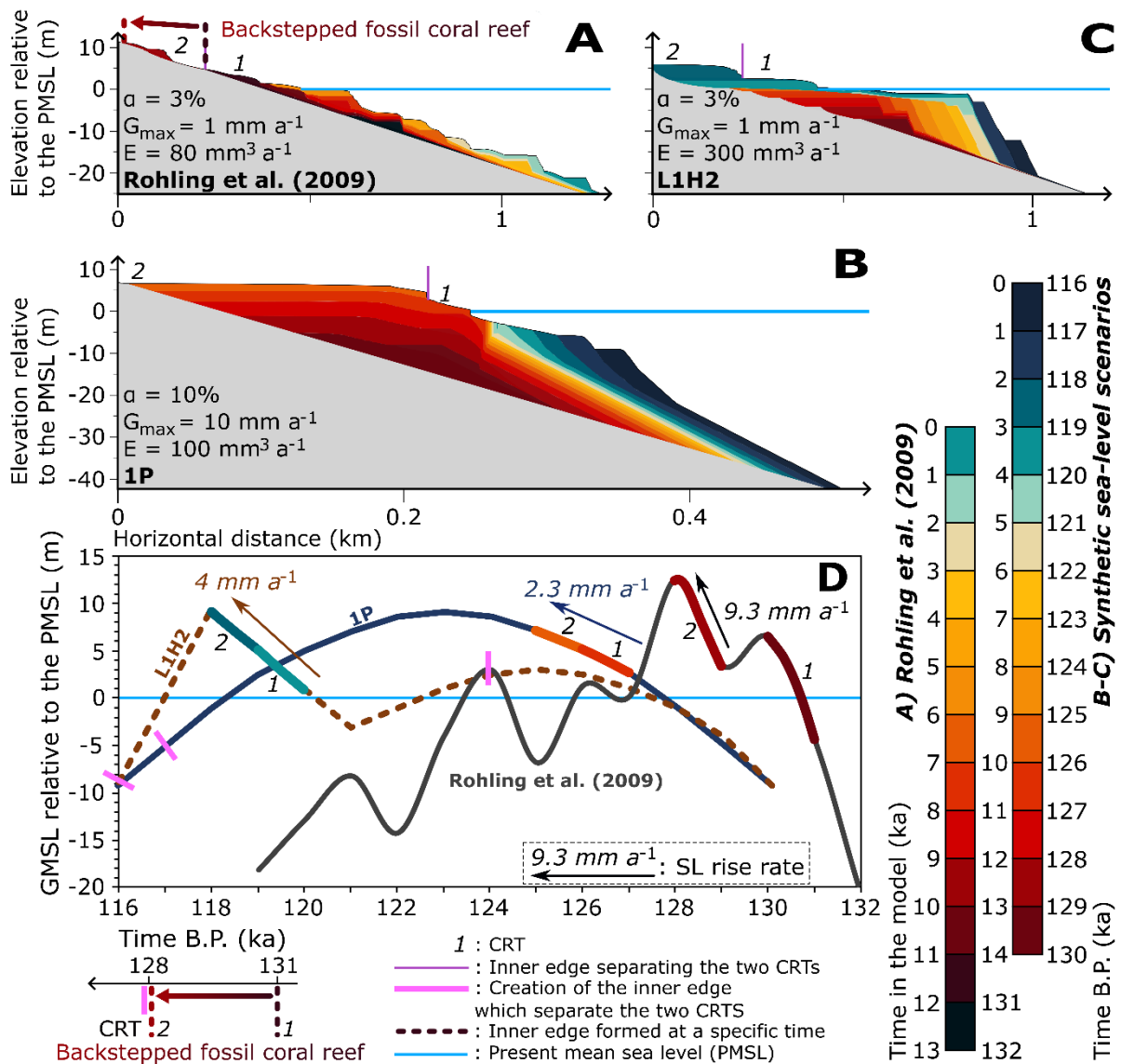
344 The inner edges are formed much later than the creation of the highest
345 CRT: 4, 8 and 2 ka later for the GMSL curve of Rohling et al. (2019), the 1P
346 and L1H2 scenarios, respectively (Figs. 5; 6). In the case of the GMSL curve
347 of Rohling et al. (2009), it is the erosion during the fourth sea-level peak
348 (124 ka ago, Fig. 5) that creates the inner edge that is now emerged (Figs.
349 5E, 5F), by eroding the coral veneer (built at 131/130 ka) as well as the
350 lowest emerged CRT (Fig. 5D).

351

352 With the 1P and L1H2 sea-level scenarios, it is the sea-level regression
353 following the maximum sea-level peak that will erode the previously
354 emerged CRT, outcropping older reefal limestone units below more recent
355 ones. For example, the long sea-level peak with a relatively stable sea level
356 of the 1P (Figs. 3B; 6D) scenario allows the construction of a large reef that
357 saturates the accommodation space from the first half of MIS 5e (up to 123
358 ka). Then, during the slow, unabrupt sea-level regression (from 123 ka;
359 Figs. 3B; 6D), the first reefal limestone unit is eroded and an older one
360 emerges. The same process applies to scenario L1H2 (Fig. 6C) but with a
361 different timing (Fig. 6D). Thus, all the inner edges generated with the 3-
362 score simulations are erosive ones. These are characterized by a time-lapse

363 that distinguishes them from the creation of the surrounding CRTs (Fig. 6D).
 364 Thus, while the sea-level rise rate seems to play an important role in the
 365 formation of backstepped reefs (Figs. 5, 6A), this does not seem to be the
 366 case for the formation of double CRTs, which is mainly explained by the
 367 action of erosion (Figs. 6B, 6C, 7).

368



369 **Figure 6.** Example of simulations that reached the maximum score of 3.
370 Simulations from the GMSL curve of **A)** Rohling et al. (2009), and the
371 synthetic sea-level scenarios **B)** 1P and **C)** L1H2 (see Fig. 2). As the model
372 does not simulate reef facies such as the reef crest, we take the inner edges
373 as the reference for the backstepping process. **D)** Sea-level scenarios listed
374 above. The pink lines mark the age at which the inner edge separating the
375 two CRTs of different ages is created. Elevations are given relative to the
376 present mean sea level (PMSL).

377

378 ***4.2. Multiple emerged CRTs (Score of 2)***

379

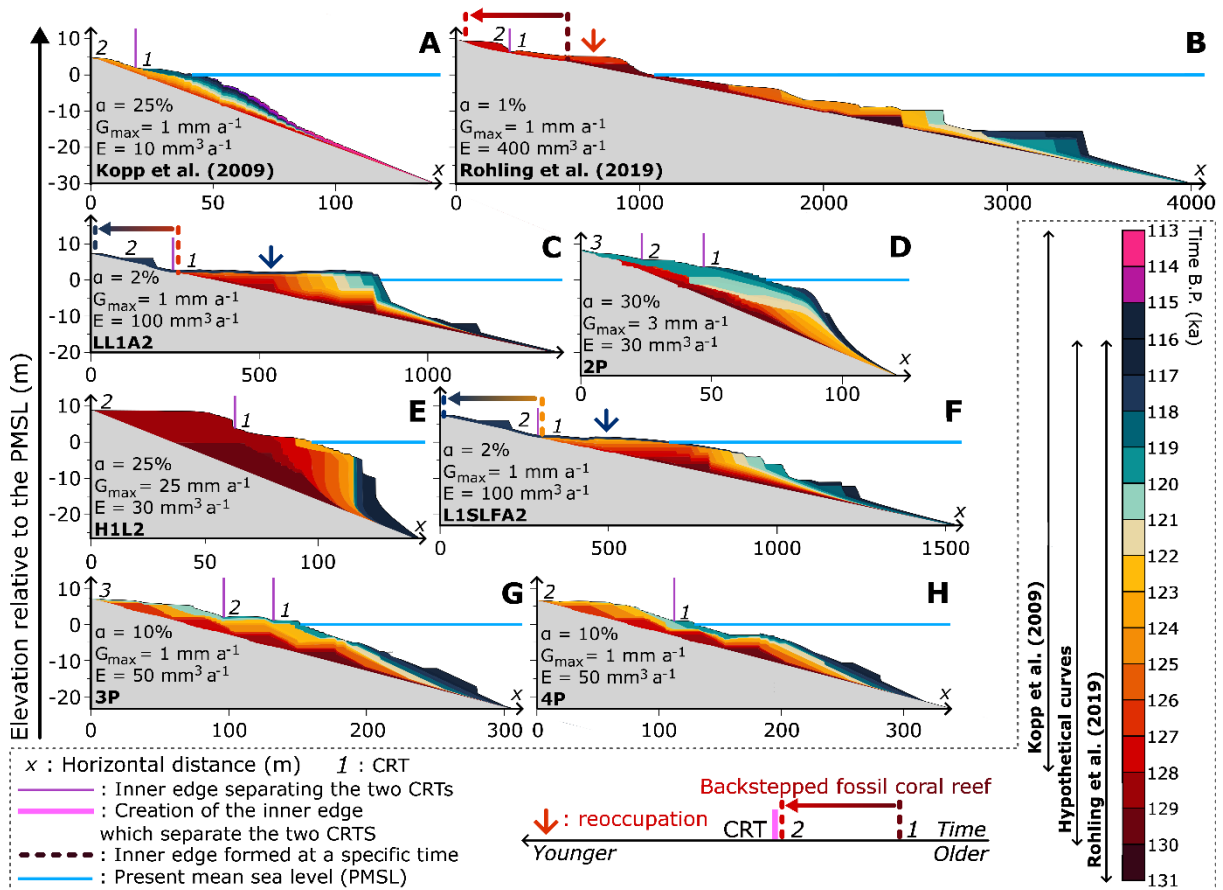
380 Of the 15 sea-level scenarios (without considering the ones of Bintanja et
381 al., 2005 and Spratt & Lisiecki, 2016), 12 have simulations with a score of
382 2, representing 16% of the total simulations. Thus, a wide range of
383 scenarios can create a multiple coral reef record: single-peak scenarios (1P,
384 LL1A2, LHP; Figs. 6; 7; SI2) as well as double/multi-peak scenarios (Kopp
385 et al., 2009, Rohling et al., 2009, 2019, 2P, L1H2, H1L2, L1SLFA2, 3P, 4P;
386 Figs. 6; 7; SI1; SI3; SI4).

387

388 This leads to a vast array of modelled reef morphologies (Fig. 7): an older
389 CRT above a more recent one, both including a single reefal limestone unit
390 (Kopp et al., 2009, LHP; Fig. 7A, 7C); a unique reefal limestone unit forming
391 two CRTs (Rohling et al., 2019, LL1A2, 2P, L1SLFA2; Fig. 7B, 7D, 7F, 7G);

392 two CRTs, each composed of several reefal limestone units (H1L2, 4P, 3P;
 393 Fig. 7F, 7I, 7H); and three distinct CRTs (2P, 3P; Fig. 7E, 7H).

394



395 **Figure 7.** Example of simulations that reached the score of 2, i.e.,
 396 simulating multiple CRTs but with an older CRT on top. Simulations from
 397 the GMSL curve of **A)** Kopp et al. (2009), **B)** Rohling et al. (2019), and the
 398 synthetic sea-level scenarios **C)** LL1A2, **D)** 2P, **E)** H1L2, **F)** L1SLFA2, **G)**
 399 3P, and **H)** 4P (see Fig. 2). As the model does not simulate reef facies such
 400 as the reef crest, we take the inner edges as the reference for the
 401 backstepping process. The color of the arrows marking the reoccupation
 402 corresponds to the time at which the reoccupation took place. Elevations
 403 are given relative to the present mean sea level (PMSL).

404

405 Three scenarios (Rohling et al., 2019; LL1A2 and L1SLFA2) have almost
406 succeeded in reproducing the backstepping process (Fig. 7B, 7D, 7F).
407 However, the last criterion was not validated because the lower CRT is
408 systematically reoccupied by a coral layer of the same age as the upper CRT
409 (Fig. 7A, 7D, 7G). In the case of the GMSL of Rohling et al. (2019), the sea-
410 level peak creating the upper backstepped reef (from 128 to 124 ka; Fig.
411 2A) is 2 ka longer than that of the GMSL of Rohling et al. (2009) (from 129
412 to 127 ka; Fig. 2A). This longer time allows the youngest reef (128-127 ka;
413 Fig. 7B) to reoccupy the oldest by a coral layer several meters thick (129-
414 128 ka; Fig. 7B), as opposed to the veneer layer constructed with the GMSL
415 curve of Rohling et al. (2009) (Fig. 5B).

416

417 The length of the highest 2nd peak is the same between the sea-level
418 scenarios LL1A2, L1SLFA2, and the GMSL of Rohling et al. (2009), i.e., 2
419 ka, and its relative elevation with respect to the lowest 1st peak differs only
420 slightly (from 5 to 6.3 m, Fig. 2A, 2B, 2C). However, the first two scenarios
421 show a reef layer reoccupying the lowest CRT (Fig. 7C, 7F), whereas the
422 last does not (Figs. 5E, 5F; 6A). This is because the LL1A2 and L1SLFA2
423 scenarios stop after the 2nd peak, whereas the GMSL curve of Rohling et al.
424 (2009) continues and experiences two further sea-level peaks above the
425 present mean sea level (at ~126 and ~124 ka, respectively, Figs. 2A; 5;
426 6D), leading to erosion of the previously formed reoccupation layer (Fig.
427 5D). As a result, with a longer and more complex eustatic history, the LL1A2
428 and L1SLFA2 scenarios would very likely have achieved a score of 3.

429

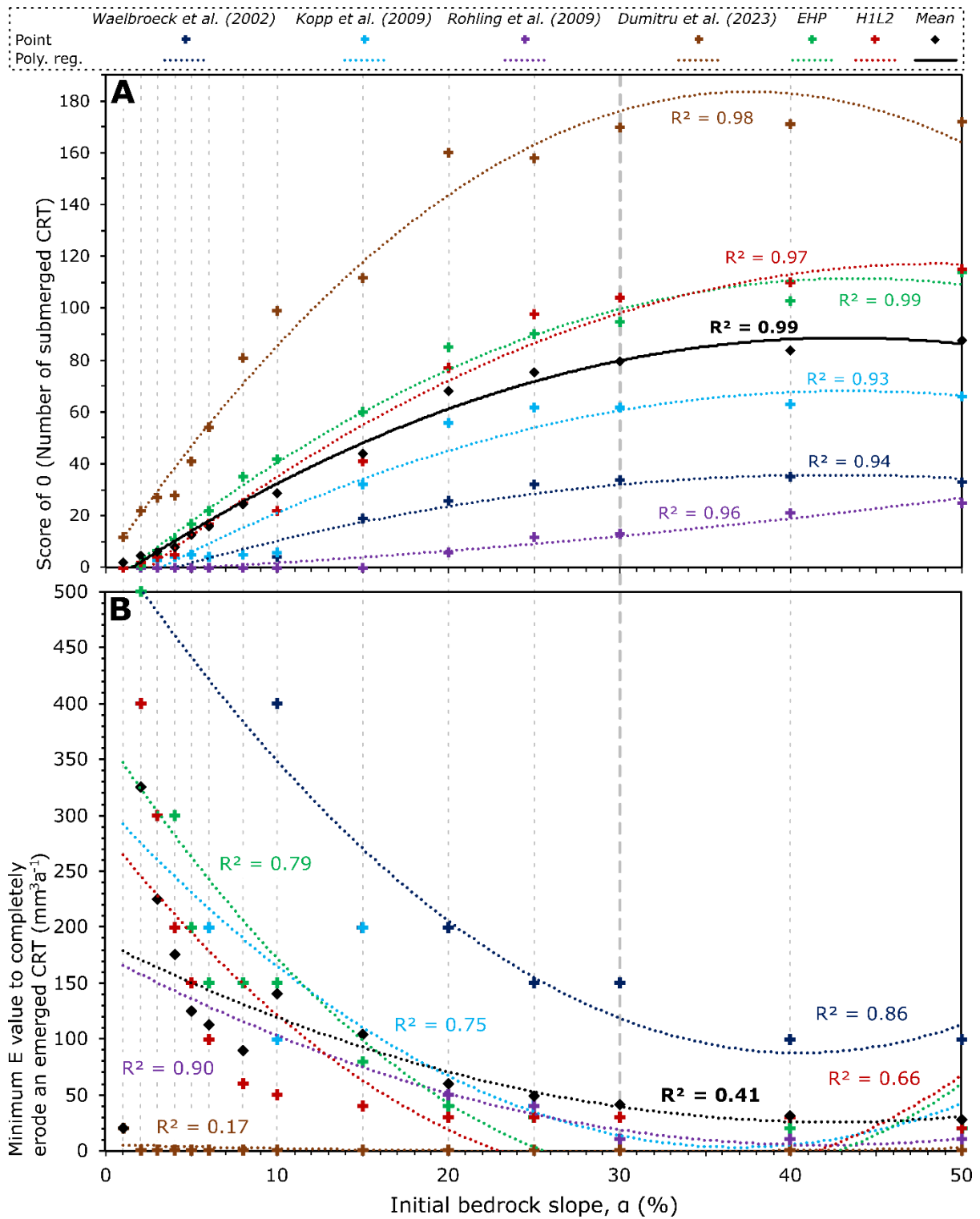
430 **4.3. Relationship between bedrock slope and marine erosion**

431

432 Our results highlight the maximum efficiency of marine erosion, which we
433 consider here as the potential of nearshore processes to erode an emerged
434 CRT. In general, marine erosion increases with the increase of the initial
435 bedrock slope α (Figs. 8; SI1; SI2; SI3; SI4). In other words, the greater
436 the bedrock slope, the more easily and quickly the emerged CRT will be
437 eroded, whatever the sea-level scenario (Fig. 8).

438

439 We note a strong correlation ($R_{\text{mean}}^2 = 0.99$) with a second-degree
440 polynomial regression between the scores of 0, or the number of submerged
441 CRTs due to marine erosion, and the bedrock slope (Fig. 8A). This
442 curvilinear relationship means an increase in the efficiency of erosion up to
443 a threshold at $\alpha = 30\%$, where the number of CRTs completely eroded no
444 longer increases significantly with the slope (Fig. 8A). The same threshold
445 is observed with the relationship between the minimum erosion rate for a
446 completely emerged CRT and the bedrock slope, i.e., the rate decreases as
447 the slope increases until it becomes stable around $\alpha = 30\%$ (Fig. 8B).



449 **Figure 8.** Relationship between marine erosion and initial bedrock slope
450 (a). **A)** Polynomial regression between the number of submerged CRT (i.e.,
451 fully eroded, score of 0) and the initial bedrock slope (α). **B)** Polynomial
452 regression between the minimum value of the marine erosion rate (E) to
453 fully erode the CRT and the initial bedrock slope (α). The relationships from
454 the synthetic sea-level scenarios 1P, LHP, LL1A2, 2P, L1H2, L1SLFA2, 3P
455 and 4P are not shown because none of the simulations from them have a
456 score of 0 or, in other words, show any completely eroded CRTs. On the
457 other hand, because no CRTs emerged at more than one meter relative to
458 the present mean sea level, the results from the GMSL curves of Bintanja
459 et al. (2005) and Spratt & Lisiecki (2016) are not considered. "Mean"
460 corresponds to the average value of the sea-level scenarios selected in
461 these relationships (i.e., Waelbroeck et al., 2002; Kopp et al., 2009; Rohling
462 et al., 2009; Dumitru et al., 2023; EHP; H1L2). The bold dotted grey line
463 marks the threshold at $\alpha = 30\%$.

464

465 **5. Discussion**

466

467 In this section, we discuss the limitations of the modelling approach we
468 employed, the realism of the parametric ranges used as input in the model,
469 and the significance of the results in terms of GMSL fluctuations during MIS
470 5e.

471

472 **5.1. Limitations**

473

474 It is important to note the limitations of the REEF model. First and foremost,
475 we assume a linear initial bedrock slope, whereas it is highly unlikely that
476 terraced landscapes begin with a linear topography. Then, the marine
477 erosion rate is based on the wave erosion model of Anderson et al. (1999).
478 It basically represents exponential wave force decay with the landward
479 distance (or decreasing depth), while most recent rock coast studies show
480 much more complicated wave transformations across platforms (e.g.,
481 considering the influence of infragravity waves on cliff retreat; Dickson et
482 al., 2013). Also, the model does not take into account subaerial erosion.
483 Moreover, the model cannot simulate the reef facies changes that are
484 observed in most of the cases of multiple reef stratigraphies (e.g., the reef
485 crest demise described by Blanchon et al., 2009 for the Yucatan Peninsula,
486 Mexico). In the same vein, we have set the maximum and optimal depths
487 for reef growth and the maximum depth of wave erosion at 20 m, 2 m, and
488 3 m respectively (Table 1), although these values can obviously vary locally.
489 Finally, the time step of the model (1 ka) prevents the study of reef
490 formation on short time scales (centennial to annual).

491

492 However, it is important to note that despite all the uncertainties of the
493 REEF model, this work is part of an ongoing international effort to develop
494 new constraints, techniques, and approaches (e.g., de Gelder et al., 2022,
495 2024; Boyden et al., 2023; Rovere et al., 2023). In addition, emerged fossil

496 coral reefs remain full-fledged geological objects which have already proven
497 their usefulness in understanding past sea-level oscillations for more than
498 a century (e.g., Darwin, 1842; Daly, 1915; Pirazzoli et al., 1991; Rovere et
499 al., 2016; Pedoja et al., 2018; Dumitru et al., 2023).

500

501 ***5.2. Real-world accuracy of parametric ranges***

502

503 The minimum value of the maximum reef growth rate used in this study
504 (i.e., $G_{\max} = 1 \text{ mm a}^{-1}$) corresponds to some shallow-water coral reefs in
505 the Caribbean and Indo-Pacific (Dullo, 2005). The maximum value of reef
506 growth rate deduced from specific reef studies is usually between 10- and
507 15-mm a^{-1} (Macintyre et al., 1977; Adey, 1978, Chappell, 1980; Davies &
508 Hopley, 1983; Bosscher & Schlager, 1992; Dullo, 2005), whereas the one
509 of this study is 50 mm a^{-1} . This high value was used to test extreme cases
510 in which the reef would consist almost exclusively of fast-growing corals
511 (e.g., *Acropora sp.*, Dullo, 2005) which saturate the accommodation space
512 (Camoin & Webster, 2015). However, we consider less realistic the
513 simulations with a maximum reef growth rate higher than 15 mm a^{-1} .

514

515 Studies using the REEF model have implemented marine erosion rate (E)
516 values ranging from 20 $\text{mm}^3 \text{ a}^{-1}$ (Pastier et al., 2019), 30 $\text{mm}^3 \text{ a}^{-1}$ (de
517 Gelder et al., 2022), 60 $\text{mm}^3 \text{ a}^{-1}$ (Chauveau et al., 2023) to 360 $\text{mm}^3 \text{ a}^{-1}$
518 (de Gelder et al., 2023). However, the lack of constraints from marine

519 erosion affecting coral reefs on millennial scales (Chauveau et al., 2021)
520 has led us to use the wide range: $E = [1-500] \text{ mm}^3 \text{ a}^{-1}$.

521

522 Initial bedrock slopes of up to 50% are likely. For example, atoll reefs can
523 grow on reef substrates with slopes close to this value (the Maldivian
524 Archipelago, Rovere et al., 2018; Pag-asa Reefs, West Philippine Sea, Janer
525 et al., 2023) but also fringing reefs (up to 25% at Cape Maisí, Cuba,
526 Authemayou et al., 2023). On the other hand, coral reefs can grow on very
527 gentle slopes (e.g., around 1/2 % for Cockburn Town reef, Bahamas, Chen
528 et al., 1991). Thus, the realism of the chosen parametric set allows us to
529 discuss with confidence the relative importance of each parameter, process,
530 and GMSL scenario on the morphogenesis of the MIS 5e coral reefs.

531

532 ***5.3. MIS 5e multiple-stepped coral reef***

533

534 Our simulations, which have a score of 2 or more (15% of the 49980
535 simulations), present two major groups: those in which the reef has not
536 saturated the accommodation space and those in which it has. The first
537 group includes backstepped reefs (whether reoccupied; Figs., 5; 6A; 7B,
538 7C, 7F) and reefs that follow sea-level changes without ever filling the
539 accommodation space (Figs. 6C; 7A, 7D, 7G, 7H). The second group
540 comprises multiple CRTs that are formed either solely by erosion (Figs. 6B;
541 7E) or by reefs built on the foreslopes of CRTs that have already emerged
542 (e.g., all the simulation with a value of $G_{\max} > 8 \text{ mm a}^{-1}$ with the 3 peaks

543 synthetic scenario, Fig. SI4). The two groups may differ completely in the
544 processes involved in reef morphogenesis, but their final morphology can
545 be very similar (Fig. 7A, 7D).

546

547 The GMSL curve of Rohling et al. (2009) is the only curve used in this study
548 to successfully simulate a younger CRT on top of an older one through a
549 backstepping process (Figs. 1; 6A). Three other scenarios were close to
550 success but failed (Rohling et al., 2019, LL1A2 and L1SLFA2; Figs. 2; 7B,
551 7C, 7F). As a result, it seems that the only eustatic explanation for creating
552 a proper emerged MIS 5e backstepped reef, in a tectonically stable area, is
553 an abrupt rise in sea level followed by a short-term peak.

554

555 The rate of this rise must be higher (at least 5 mm a^{-1} in our study, LL1A2
556 scenario, Fig. 2B) than the local reef growth rate (no more than 1 mm a^{-1}
557 in our study, Figs. 6A; SI1) to drown the first CRT (Camoin & Webster,
558 2015). The second peak must be short to avoid any reoccupation of the first
559 CRT (no more than 2 ka in our study, Section 4.1., Fig. 7), as must the
560 following regression so as not to completely erode it.

561

562 A drop in sea level between the two peaks (as at 118 ka with the L1SLFA2
563 scenario, Fig. 2C) seems counter-productive to reproduce a backstepped
564 fossil reef because, during it, the previously emerged CRT will be potentially
565 eroded. To our knowledge, the site near Xcaret (Yucatan, Mexico; Blanchon
566 et al., 2009; Blanchon, 2010) is the only one outcropping a MIS 5e

567 backstepped reef in a stable area. As a result, the MIS 5e backstepped reefs
568 simulated with the REEF model (Figs. 5; 6A; 7B, 7C, 7F) appear to have
569 only this real equivalent.

570

571 For the other two scenarios that reach a score of 3, L1H2 and 1P, it is not
572 GMSL fluctuation that entirely explains the formation of a younger CRT on
573 top of an older one, but mostly marine erosion. More specifically, its
574 capacity to dismantle reefal limestone units and cause older ones to emerge
575 (Chauveau et al., 2021; Stout et al., 2023), specifically during sea-level
576 regression (Fig. 6B, 6C, 6D; Chauveau et al., 2023).

577

578 To conclude, a wide range of sea-level scenarios can form multiple
579 stratigraphies with an equally wide range of processes: GMSL fluctuations
580 (Figs., 6A; 7B, 7C, 7F) and marine erosion (Fig., 6B), or the combination of
581 both (Figs., 6C; 7A, 7D, 7E, 7G, 7H). This approach aligns with the recent
582 contributions of Georgiou et al. (2024) who extracted diverse sea-level
583 scenarios through the simulation of erosional RSL indicators (i.e. tidal notch
584 geometry) by combining various parameters affecting their development.
585 Although we cannot conclude whether there were abrupt changes in GMSL
586 during the MIS 5e, we can state that **1)** the GMSL at MIS 5e must have
587 been higher than 2 m (= the optimal reef growth depth, Table 1) to build
588 reefs that are now emerged in tectonically stable areas and **2)** that marine
589 erosion should be systematically considered when establishing the chrono-
590 stratigraphy of fossil coral reefs and the resulting RSL reconstructions.

591

592 **6. Conclusion**

593

594 It is crucial to constrain the rate of the very likely future sea-level rise. One
595 of the keys to this is to study past interglacial periods, the last of which is:
596 the Marine Isotope Stage 5e. The global mean sea level at that time may
597 well have fluctuated rapidly, as numerous multiple-stepped stratigraphies
598 around the world seem to testify. These come particularly from fossil coral
599 reefs in tectonically stable areas.

600

601 Here, by meticulously analyzing nearly 50 thousand simulations from a coral
602 reef evolution numerical model, we assess the realistic parametric
603 conditions and sea-level scenarios under which such stratigraphies can be
604 generated. Although this model has some limitations, our results show that
605 the only eustatic explanation for emerged backstepped fossil coral reefs (as
606 in the Yucatan Peninsula, Mexico) is a first sea-level peak followed by a
607 period of stabilization or decline, an abrupt rise in sea level and a second
608 short-term peak. There is no need, however, to invoke such abrupt sea-
609 level fluctuations to form other types of multiple-stepped coral reef
610 stratigraphy. Indeed, we emphasize the interactions between bedrock
611 slope, reef growth, and marine erosion. The latter can be a major shaping
612 agent, as it can strip recent reefal limestone units to expose older ones,
613 leading to chrono-morpho-stratigraphies that can be misinterpreted.

614 Finally, all the conclusions drawn in this study could be improved by further
615 analyses using stratigraphic forward models for specific sites.

616

617 **Acknowledgements**

618

619 This project has received funding from the European Research Council
620 (ERC) under the European Union's Horizon 2020 research and innovation
621 programme (grant agreement No.802414). We would like to thank Dr.
622 Anne-Morwenn Pastier for her explanations and help with the REEF model
623 and for the fruitful discussions. With regard to the image shown in Figure
624 1A, we would like to thank the following projects (conducted by Dr. Christine
625 Authemayou) which enabled Dr. Denovan Chauveau to carry out fieldwork
626 in south-east Cuba and take this photography: "This fieldwork was
627 supported by public funds received in the framework of GEOSUD
628 (DINAMIS), a project (ANR-10-EQPX-20) of the program "*Investissements*
629 *d'Avenir*" managed by the French National Research Agency. It was also
630 supported by the ISblue project, Interdisciplinary graduate school for the
631 blue planet (ANR-17-EURE-0015) and co-funded by a grant from the French
632 government under the program "*Investissements d'Avenir*" embedded in
633 France 2030 (VuCoRem project, C. Authemayou) and the CNES TOSCA
634 program (CETTROPICO, C. Authemayou)."

635

636 **Supplementary Information**

637

638 All 49980 simulations analyzed in this study as well as the scoring
639 spreadsheets for each sea-level scenario are available in a ZENODO
640 repository (<https://doi.org/10.5281/zenodo.10695610>). A description of
641 the published GMSL curves used in this study can be found in Section SI.1.
642 A description of all the simulations output by the model can be found in
643 Section SI.2. We separated those obtained from proxy-based GMSL
644 scenarios (Section SI.2.1.) from those obtained with the synthetic sea-level
645 curves (Section SI.2.2.). We also present four figures (Figs. SI1; SI2; SI3;
646 SI4) showing the overall scores for each of the 44100 simulations analyzed
647 here.

648

649 **Supplementary Information**

650

651 ***SI.1. Description of the proxy-based global mean sea level curves***

652

653 The reconstruction of Waelbroeck et al. (2002) is based on oxygen isotopic
654 ratios of benthic foraminifera from the North Atlantic and Equatorial Pacific
655 Ocean over the last 430 ka and calibrated with the elevation of coral
656 samples corrected from vertical deformation. Thus, Waelbroeck et al.
657 (2002) provide the result of a compilation of several proxies from different
658 parts of the global ocean. Bintanja et al. (2005) used numerical modelling
659 to reconstruct GMSL variations and continental ice volume over 1 Ma from
660 a continuous global compilation of benthic oxygen isotope data. With an
661 extensive compilation of local sea-level indicators (42 localities) and a

662 statistical approach, Kopp et al. (2009) estimated the GMSL from 140 to 90
663 ka ago. Rohling et al. (2009) used the oxygen isotopic ratios of planktonic
664 foraminifera and bulk sediment from the central Red Sea over 520 ka, while
665 inferring those local variations are roughly representative of GMSL. The
666 meta-analysis of Spratt & Lisiecki (2016) is based on a principal component
667 analysis of earlier compilations (Bintanja et al., 2005; Elderfield et al.,
668 2012; Rohling et al., 2009; Rohling et al., 2014; Shakun et al., 2015;
669 Sosdian & Rosenthal, 2009; Waelbroeck et al., 2002), up to 800 ka. To
670 translate the continuous single-core RSL record of central Red Sea KL11
671 core (also used in Rohling et al. 2009) to GMSL and to quantify the AIS
672 contributions, Rohling et al. (2019) authors applied apply a first order
673 glacio-isostatic correction and subtract the GIS contribution records (from
674 Yau et al., 2016). Dumitru et al. (2023) presented a RSL MIS 5e record
675 based on high-precision U-series ages of 23 corals collected in the Bahamas
676 archipelago (Crooked Island, Long Cay, Long Island, and Eleuthera). After
677 a strict screening criteria selection of the samples, these authors inferred
678 GMSL from these local data by correcting them for GIA and long-term
679 subsidence (considering a range of ice histories and Earth viscosity
680 structures).

681

682 ***SI.2. Description of all the model outputs.***

683 ***SI.2.1. Proxy-based GMSL scenarios***

684

685 The simulations derived from the GMSL curve of Waelbroeck et al. (2002)
686 achieve a maximum score of 1 in the 94% of cases. This means that, with
687 this sea-level scenario, the model did not reproduce any double CRT over
688 the range of parameters used. We note that with a slope of 10% or more
689 and relatively high maximum reef growth rate (G_{\max}) and marine erosion
690 rate (E) values, no fossil reefs emerge because they are completely eroded
691 (Fig. SI1). None of the simulations from the GMSL curves of Bintanja et al.
692 (2005) and Spratt & Lisiecki (2016) reach a score higher than 0. This
693 happens because the maximum peak of these curves is less than 1 m
694 relative to present mean sea level, and therefore less than our limit of 1 m
695 for considering a CRT as emerged (Fig. 1B).

696

697 The maximum score reached by the simulations using as sea-level input the
698 GMSL from Kopp et al. (2009) is 2 (Fig. SI1). In fact, while 838 out of 2940
699 simulations (29%) using this sea-level scenario reproduce multiple CRTs,
700 no simulation originates a younger reef unit above an older one (Fig. SI1).
701 Within the simulations with a score of 2, multiple coral reef morphologies
702 are created only when reef erosion rates (E) fall below $100 \text{ mm}^3 \text{ a}^{-1}$. Reef
703 growth rates (G_{\max}) do not seem to influence in a significant way the
704 scoring, however higher scores are generally achieved with higher rates
705 ($10\text{-}50 \text{ mm a}^{-1}$). From $\alpha = 2\%$, the emerged CRT starts to disappear (i.e.,
706 simulations with a score of 0 are starting to output, Fig. SI1). Scores of 0
707 are first concentrated at $G_{\max} = 1 \text{ mm a}^{-1}$ up to $\alpha = 8\%$, then gradually
708 widens to all G_{\max} values at $\alpha = 50\%$.

709

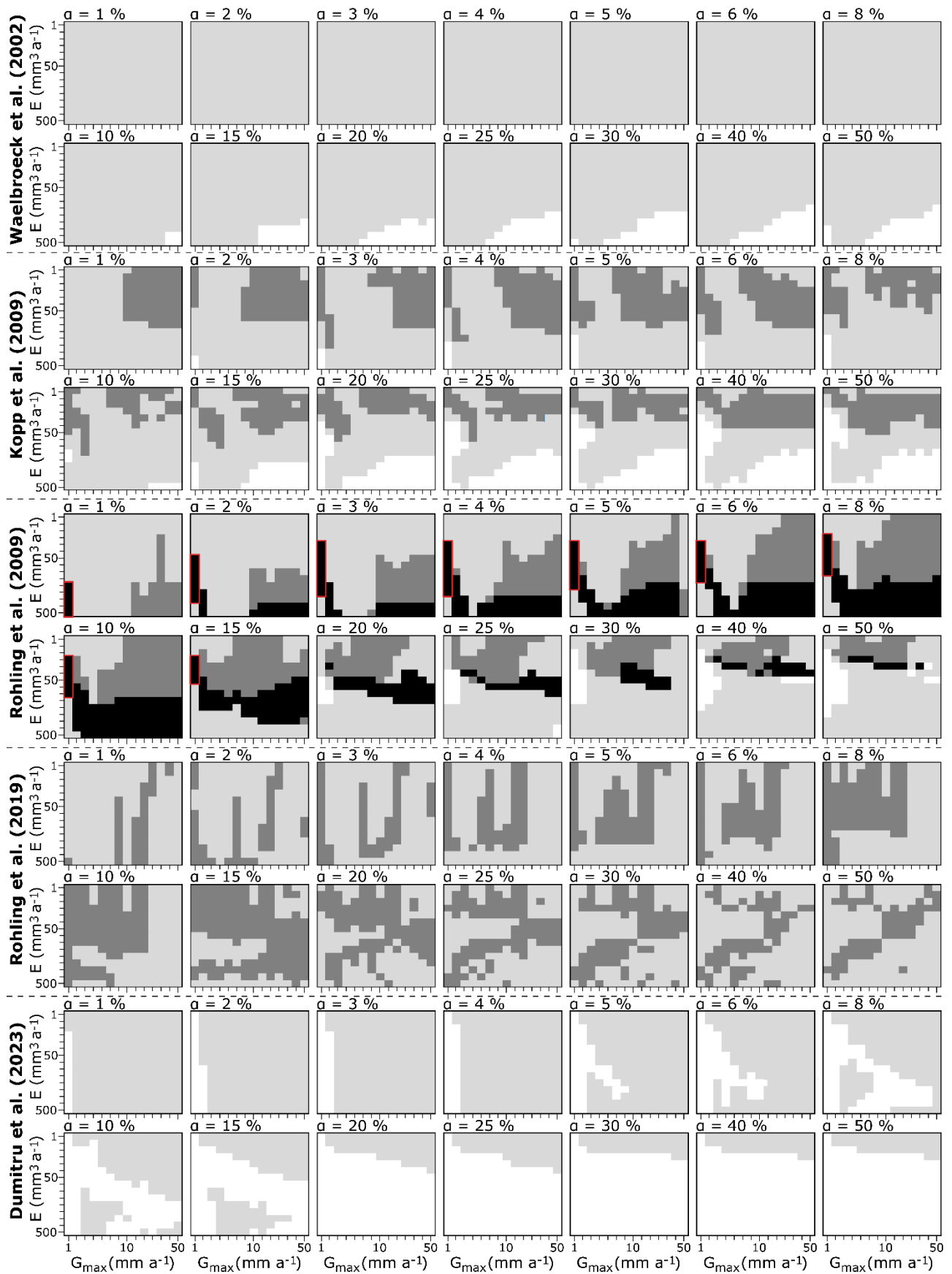
710 Over 2940 simulations using the sea-level curve of Rohling et al. (2009),
711 523 (18%) attain the highest possible scoring (i.e., 3, Fig. SI1). This score
712 is reached over the entire range of bedrock slopes (α), reef growth rates
713 (G_{\max}), and when reef erosion (E) is between 20 to 500 $\text{mm}^3 \text{a}^{-1}$ (Fig. SI1).
714 Simulations with a score of 2 cover the whole range of G_{\max} and E , and from
715 α between 5% to 10%. As the slope and erosion rate increase, the model
716 starts to output more simulations with one single emerged CRT (score of 1,
717 Fig. SI1). Simulations with a score of 0 (no emerged CRT) start at $\alpha = 20\%$
718 and for values of $E = [50-100] \text{mm}^3 \text{a}^{-1}$ and $G_{\max} = [1,2] \text{mm} \text{a}^{-1}$. Scores of
719 0 increase gradually as α increases. In the end, almost half of the
720 simulations (i.e., 43%) have scores of either 2 or 3, which means that they
721 are characterized by multiple coral reef units during the MIS 5e.

722

723 Although the Rohling et al. (2019) GMSL curve is very similar to that of
724 Rohling et al. (2009) (Fig. 2A), the first does not reach a score of 3 (Fig.
725 SI1). This is because the first sea-level peak of the GMSL curve of Rohling
726 et al. (2019) curve (from 128 to 124 ka; Fig. 2A) is 2 ka longer than that
727 of GMSL curve of Rohling et al (2009) (from 129 to 127 ka; Fig. 2A), leading
728 to a systematic reoccupation of the older low terrace (aged of 130-129 ka)
729 by a younger reef (aged of 127/126 ka; Fig. 5B). This therefore invalidates
730 criterion 3 (See Section 4.2. of the main manuscript for further
731 explanation). Although scores of 2 represent 38% of the total simulations,
732 no clear trend emerges (Fig. SI1).

733

734 For the GMSL curve of Dumitru et al. (2023), the maximum score is 1 (Fig.
735 SI1), which is reached in 56% of simulations. Simulations with scores of 0
736 start at $\alpha = 1\%$ but only at $G_{\max} = 1 \text{ mm a}^{-1}$. These increase to higher G_{\max}
737 values as the slope increases. From $\alpha = 20\%$, there are only a few
738 simulations with a score of 1 (Fig. SI1).



Score **0 1 2 3**

Backstepped fossil coral reef

740 **Figure SI1.** Parametric study of the simulations from published/proxy-based GMSL
741 curves. GMSL curves scenarios (rows), initial bedrock slopes (α , rows and columns),
742 maximum reef growth rates (G_{max} ; x axis) and erosion rates (E ; y axis). The color of
743 each “small box” represents the score of the simulation for a given parametrization
744 based on the chrono-morphological criteria defined in section 3. Each “medium box”
745 shows simulation scores for the range of G_{max} , and the range of E . Each line of
746 “medium boxes” shows the variability along the range of α . The simulations with a
747 score of 3 correspond to a black square. The results from the GMSL scenarios of
748 Bintanja et al. (2005) and Spratt & Lisiecki (2016) are not shown because none of the
749 simulations derived from them have a score higher than 0.

750

751 **SI.2.2. Synthetic SL curves**

752

753 Here, we describe the results for each synthetic sea-level scenario, i.e.,
754 Single- Double- Multi-peak group scenarios (respectively Figs. SI2, SI3, and
755 SI4).

756

757 **SI.2.2.1. Single-peak scenarios**

758

759 The maximum score achieved by the one major peak (1P, Fig. 2B) scenario
760 is 3, which is achieved in 6% of the simulations under this sea-level pattern
761 (Fig. SI2). This score is achieved from $\alpha = 5\%$ to 50% . From $\alpha = 8\%$ to
762 15% , the scores of 3 cover almost the entire G_{max} range (i.e., $G_{max} = [2-$
763 $50] \text{ mm a}^{-1}$ for $\alpha = 10\%$), narrowing to $G_{max} = [1-3] \text{ mm a}^{-1}$ from $\alpha = 25\%$.
764 Regarding the erosion rate, the maximum scores are constrained to $E =$

765 [80-300] mm³ a⁻¹ for α = [5-8]% and then to the range E = [20-300] mm³
766 a⁻¹ for higher α values (Fig. SI2). Scores of 2 represent only 3% (81
767 simulations) of the 2940 simulations (Fig. SI2), while scores of 1 represent
768 91% (2676 simulations).

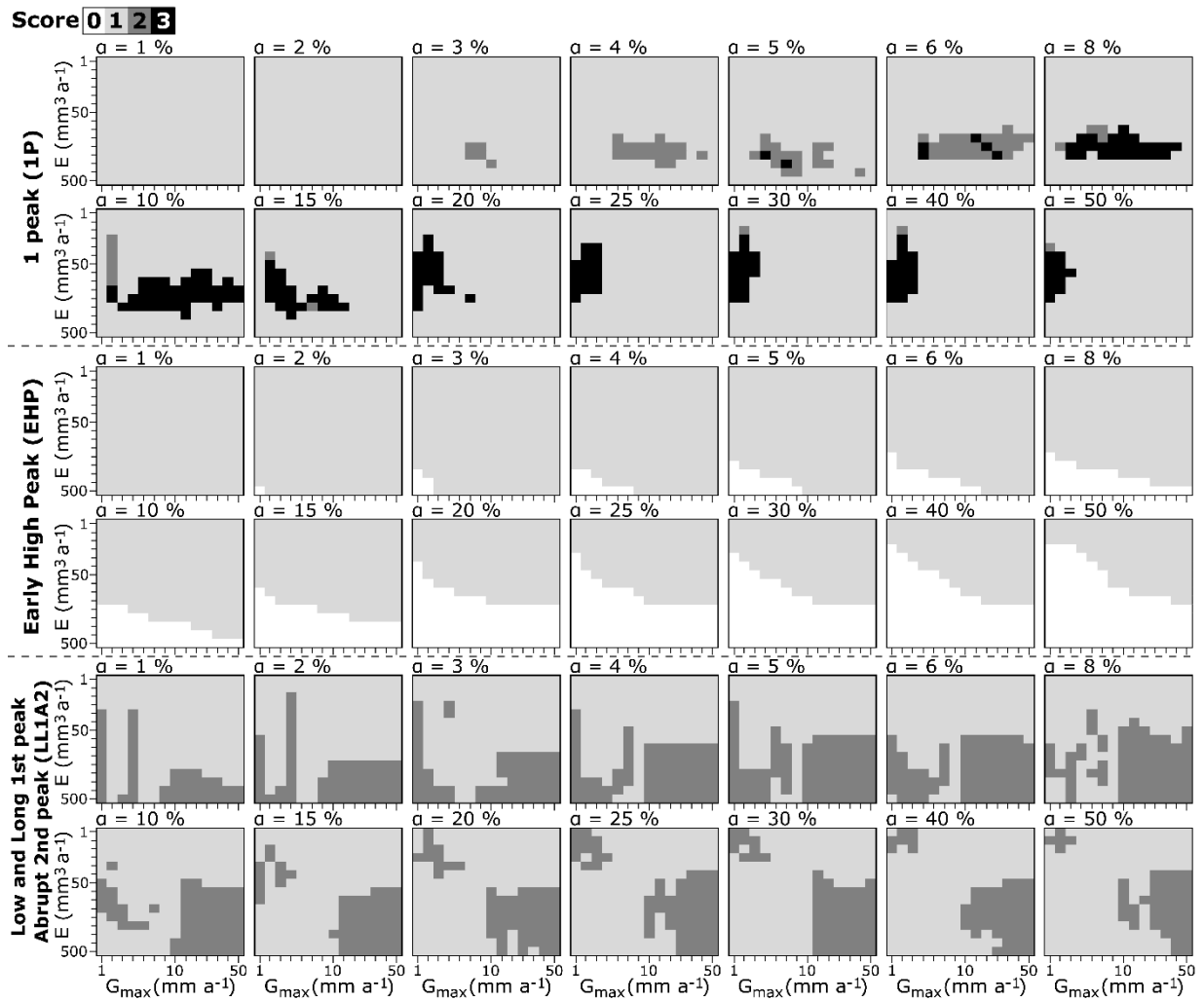
769

770 All the simulations using the Late High Peak (LHP) scenario have a score of
771 1. This means that, only one emerged CRT is modelled under this scenario.

772

773 With an Early High Peak (EHP) the maximum score attained is 1 (Fig. SI2),
774 in 77% of our model runs (2260 simulations). This score represents all
775 simulations at α = 1%. From α = 2%, the model simulates a score of 0 at
776 $G_{\max} = 1$ mm a⁻¹ and E = 500 mm³ a⁻¹. There are more and more 0 scores
777 as α increases. Thus, simulations with a score of 0 represent 54% of all
778 simulations at α = 50%.

779



780 **Figure SI2.** Parametric study of the simulations from the synthetic GMSL curves of the
 781 single-peak scenario group. Same description as Figure SI1. The results from the Late
 782 High Peak (LHP) scenario are not shown because none of the simulations derived from
 783 it have a score different than 1.

784

785 Under the sea-level scenario characterized by a Low and Long 1st peak and
 786 an abrupt 2nd peak (LL1A2), a score of 2 is attained in 31% of our model
 787 runs (921 simulations), while 61% of simulations reach a score of 1 (2019
 788 simulations). The simulations are divided in two groups from $\alpha = 1\%$. The
 789 first group is constrained to $G_{\max} < 6/8 \text{ mm a}^{-1}$, the second concentrated

790 on values of $G_{\max} > 6/8 \text{ mm a}^{-1}$ and $E > 40 \text{ mm}^3 \text{ a}^{-1}$. These two groups
791 become more distinct as α values increase (Fig. SI2).

792

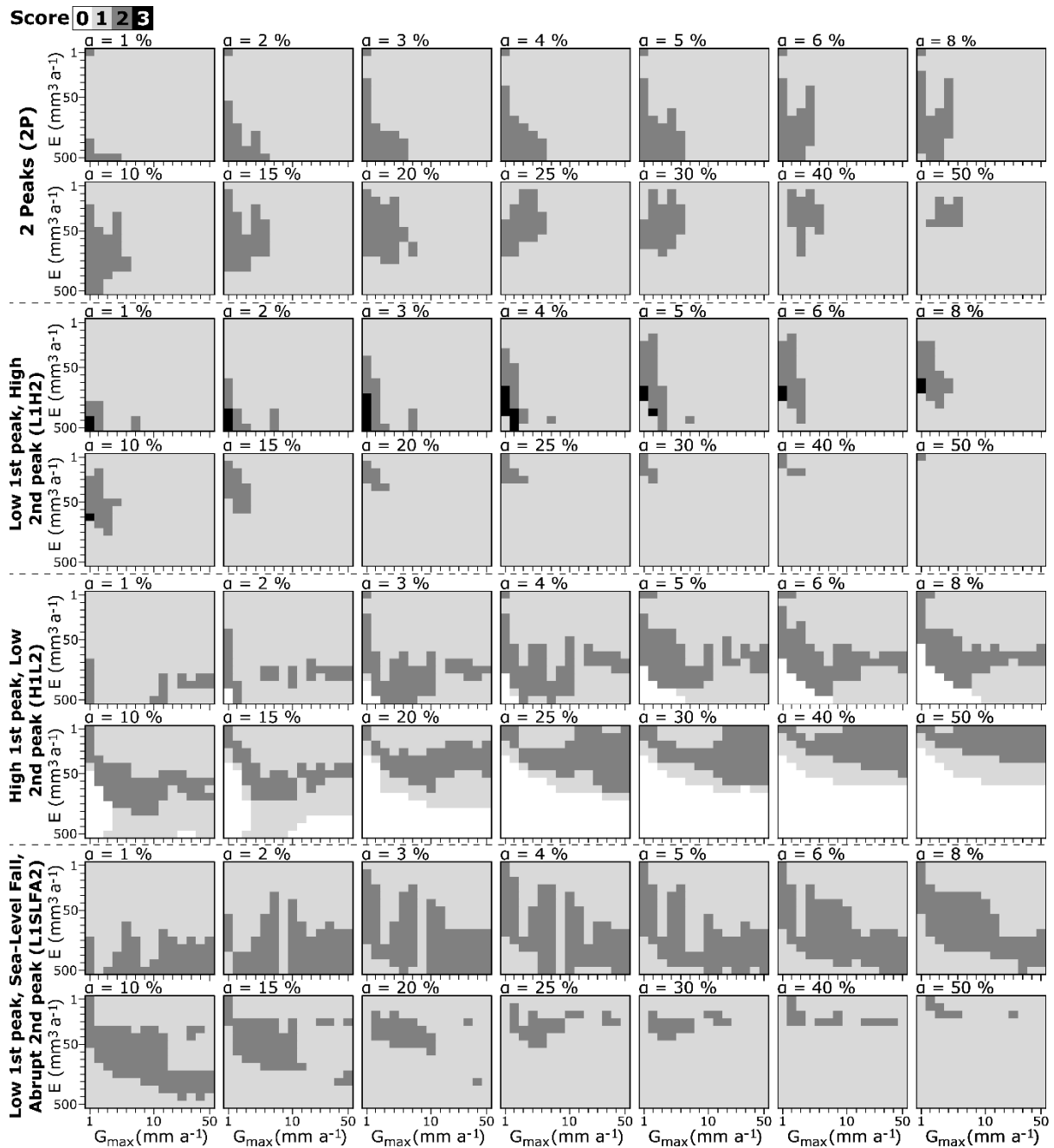
793 ***SI.2.2.2. Double-peak scenarios***

794

795 The maximum score of 2 is reached for the two-peaks (2P) sea-level
796 scenario (13% of the total; Fig. SI3). These scores are concentrated around
797 $E = 500 \text{ mm}^3 \text{ a}^{-1}$ and low G_{\max} values (under 5 mm a^{-1}) at $\alpha = 1\%$. The
798 number of 2-scores increase as the α increases. From $\alpha = 15\%$, there are
799 no longer any simulations with a score of 2 at $E = 500 \text{ mm}^3 \text{ a}^{-1}$. This trend
800 continues at lower erosion rate values until $E = 50 \text{ mm}^3 \text{ a}^{-1}$ for $\alpha = 50\%$.
801 Also, from $\alpha = 40\%$, there are no more scores of 2 at $G_{\max} = 1 \text{ mm a}^{-1}$. The
802 score of 3 has almost been reached by 2P, with a younger reefal limestone
803 unit sometimes emerging above an older one, but the separation between
804 the two is not morphologically significant enough to consider that they form
805 two distinct units.

806

807 The maximum score of 3 is reached by the Low 1st peak, High 2nd peak (i.e.,
808 L1H2) scenario (1% of total; Fig. SI3). These scores are only concentrated
809 at $G_{\max} = [1,2] \text{ mm a}^{-1}$ and at $E > 80 \text{ mm}^3 \text{ a}^{-1}$. The scores of 2 seem to
810 show the same trend as those of scenario 2P, i.e., concentrated almost over
811 the whole E range and $G_{\max} = [1-6] \text{ mm a}^{-1}$ from $\alpha = [1-5] \%$. There are
812 fewer and fewer scores of 2 as α increases. At $\alpha = 50\%$ only 1 simulation
813 with a score of 2 remain.



815 **Figure SI3.** Parametric study of the simulations from the synthetic GMSL curves of the
 816 double-peak scenario group. Same description as Figure SI1.

817

818 A maximum score of 2 is attained for the High 1st peak, Low 2nd peak (H1L2)
 819 scenario (Fig. SI3). The 2-score simulations are dispersed across the ranges
 820 of E and G_{\max} . These are concentrated around $E = [100-500] \text{ mm}^3 \text{ a}^{-1}$ at α
 821 $= 1\%$, whereas they are partitioned around $E = [1-30] \text{ mm}^3 \text{ a}^{-1}$ at $\alpha = 50\%$.

822 At $\alpha = 2\%$, there are two simulations with a score of 0 (Fig. SI3). The
823 number of simulations with a score of 0 increases as the slope increases. At
824 $\alpha = 50\%$, these scores represent 55% of the 210 simulations (Fig. SI3).

825

826 The last sea-level scenario of group II (i.e., Low 1st peak, Sea-Level Fall,
827 Abrupt 2nd peak, L1SLFA2), attained the maximum score of 2 (Fig. SI3).

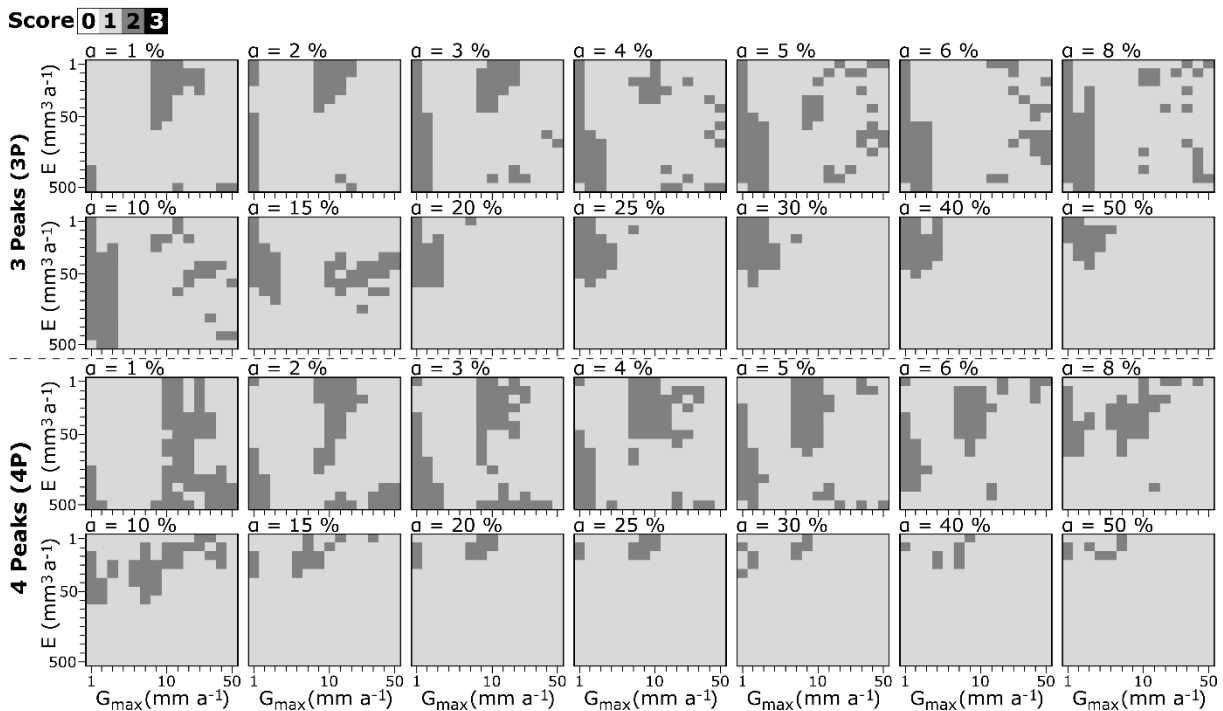
828 These scores are concentrated for almost all G_{\max} value ranges and below
829 $E = 80 \text{ mm}^3 \text{ a}^{-1}$ at $\alpha = 1\%$. The number of simulations with a score of 2
830 decreases as α values increase. Thus, the scores of 1 represent almost the
831 entire range of simulation at $\alpha = 50\%$ ($\sim 95\%$ of the 210 simulations, Fig.
832 SI3).

833

834 **SI.2.2.3. Multi-peak scenarios**

835

836 The maximum score of 3 is not reached by either the 3-peaks (3P) or 4-
837 peaks (4P) scenario, only scores of 1 and 2 (Fig. SI4). For the 3P scenario,
838 there are two distinct groups of 2-scores (525 simulations, 18% of total)
839 for values of $\alpha = [1-15] \%$, one concentrated on values of $G_{\max} < 8 \text{ mm a}^{-1}$
840 and the other at $G_{\max} > 8 \text{ mm a}^{-1}$. At $\alpha > 15 \%$, the scores of 2 are
841 concentrated at $G_{\max} < 5 \text{ mm a}^{-1}$ and $E < 60 \text{ mm}^3 \text{ a}^{-1}$. For the 4P scenario,
842 scores of 2 (477 simulations, 16% of total) also seem to form the same two
843 groups as those highlighted by 3P (Fig. SI4).



845 **Figure S14.** Parametric study of the simulations from the synthetic GMSL curves of the
 846 multi-peak scenario group. Same description as Figure S11.

847

848 References

849

850 **1.** Adey W (1978) Coral reef morphogenesis: a multi-dimensional model.
 851 Science 202:831–837.

852

853 **2.** Anderson, R.S., Densmore, A.L. & Ellis, M.A. (1999) The generation
 854 and degradation of marine terraces. Basin Research, 11(1), 7–20.
 855 Available from: <https://doi.org/10.1046/j.1365-2117.1999.00085.x>

856

857 **3.** Authemayou, C., Nuñez, A., Pedroja, K., Peñalver, L., Chauveau, D.,
 858 Dunán-Avila, P., ... & Anne-Morwenn, P. (2023). Oblique collision of

859 the Bahamas platform at the northern boundary of the Caribbean
860 Plate recorded by the late Cenozoic coastal terraces of SE Cuba.
861 Tectonics, 42(8). <https://doi.org/10.1029/2023TC007806>
862

863 **4.** Barlow, N. L., McClymont, E. L., Whitehouse, P. L., Stokes, C. R.,
864 Jamieson, S. S., Woodroffe, S. A., ... & Sanchez-Montes, M. L. (2018).
865 Lack of evidence for a substantial sea-level fluctuation within the Last
866 Interglacial. *Nature Geoscience*, 11(9), 627-634.
867

868 **5.** Barnett, R. L., Austermann, J., Dyer, B., Telfer, M. W., Barlow, N. L.,
869 Boulton, S. J., ... & Creel, R. C. (2023). Constraining the contribution
870 of the Antarctic Ice Sheet to Last Interglacial sea level. *Science*
871 *Advances*, 9(27), eadf0198.
872

873 **6.** Blanchon, P. (2010). Reef demise and back-stepping during the last
874 interglacial, northeast Yucatan. *Coral Reefs*, 29(2), 481-498.
875

876 **7.** Blanchon, P., Eisenhauer, A., Fietzke, J., & Liebetrau, V. (2009).
877 Rapid sea-level rise and reef back-stepping at the close of the last
878 interglacial highstand. *Nature*, 458(7240), 881-884.
879

880 **8.** Bintanja, R., Van De Wal, R. S., & Oerlemans, J. (2005). Modelled
881 atmospheric temperatures and global sea levels over the past million
882 years. *Nature*, 437(7055), 125-128.

883

884 **9.** Bosscher, H. & Schlager, W. (1992) Computer simulation of reef
885 growth. *Sedimentology*, 39(3), 503–512. Available from:
886 <https://doi.org/10.1111/j.1365-3091.1992.tb02130.x>

887

888 **10.** Boyden, P., Weil-Accardo, J., Deschamps, P., Godeau, N., Jaosedy,
889 N., Guihou, A., ... & Rovere, A. (2022). Revisiting battistini:
890 Pleistocene coastal evolution of southwestern madagascar. *Open*
891 *Quaternary*, 8(1), 1-17.

892

893 **11.** Bruggemann, J. H., Buffler, R. T., Guillaume, M. M., Walter, R. C., von
894 Cosel, R., Ghebretensae, B. N., & Berhe, S. M. (2004). Stratigraphy,
895 palaeoenvironments and model for the deposition of the Abdur Reef
896 Limestone: context for an important archaeological site from the last
897 interglacial on the Red Sea coast of Eritrea. *Palaeogeography,*
898 *Palaeoclimatology, Palaeoecology*, 203(3-4), 179-206.

899

900 **12.** Camoin, G. F., & Webster, J. M. (2015). Coral reef response to
901 Quaternary sea-level and environmental changes: State of the
902 science. *Sedimentology*, 62(2), 401-428.

903

904 **13.** Chappell, J. *Geology of Coral Terraces, Huon Peninsula, New Guinea:*
905 *A Study of Quaternary Tectonic Movements and Sea- sevel Changes.*
906 *GSA Bulletin* 85, 553–570 (1974).

907

908 **14.** Chappell, J. (1980). Coral morphology, diversity and reef growth.
909 Nature, 286(5770), 249-252.

910

911 **15.** Chauveau, D., Authemayou, C., Pedoja, K., Molliex, S., Husson, L.,
912 Scholz, D., ... & Aster Team. (2021). On the generation and
913 degradation of emerged coral reef terrace sequences: First
914 cosmogenic ³⁶Cl analysis at Cape Laundi, Sumba Island (Indonesia).
915 Quaternary Science Reviews, 269, 107144.
916 <https://doi.org/10.1016/j.quascirev.2021.107144>

917

918 **16.** Chauveau, D., Pastier, A. M., de Gelder, G., Husson, L., Authemayou,
919 C., Pedoja, K., & Cahyarini, S. Y. (2023). Unravelling the
920 morphogenesis of coastal terraces at Cape Laundi (Sumba Island,
921 Indonesia): insights from numerical models. Earth Surface Processes
922 and Landforms. <https://doi.org/10.1002/esp.5720>

923

924 **17.** Chen, J. H., Curran, H. A., White, B., & Wasserburg, G. J. (1991).
925 Precise chronology of the last interglacial period: ²³⁴U-²³⁰Th data
926 from fossil coral reefs in the Bahamas. Geological Society of America
927 Bulletin, 103(1), 82-97.

928

929 **18.** Chutcharavan, P. M., & Dutton, A. (2021). A global compilation of U-
930 series-dated fossil coral sea-level indicators for the Last Interglacial

- 931 period (Marine Isotope Stage 5e). *Earth System Science Data*, 13(7),
932 3155-3178.
- 933
- 934 **19.** Davies, P., Hopley, D. (1983) Growth facies and growth rates of
935 Holocene reefs in the Great Barrier Reef. *BMR J Austr Geol Geophys*
936 8:237–251
- 937
- 938 **20.** DeConto, R. M., Pollard, D., Alley, R. B., Velicogna, I., Gasson, E.,
939 Gomez, N., ... & Dutton, A. (2021). The Paris Climate Agreement and
940 future sea-level rise from Antarctica. *Nature*, 593(7857), 83-89.
- 941
- 942 **21.** Deiana, G., Antonioli, F., Moretti, L., Orrù, P. E., Randazzo, G., & Lo
943 Presti, V. (2021). MIS 5.5 highstand and future sea level flooding at
944 2100 and 2300 in tectonically stable areas of central Mediterranean
945 Sea: Sardinia and the Pontina Plain (Southern Latium), Italy. *Water*,
946 13(18), 2597.
- 947
- 948 **22.** de Gelder, G., Jara-Munoz, J., Melnick, D., Fernández-Blanco, D.,
949 Rouby, H., Pedoja, K., ... & Lacassin, R. (2020). How do sea-level
950 curves influence modeled marine terrace sequences?. *Quaternary*
951 *Science Reviews*, 229, 106132.
- 952
- 953 **23.** de Gelder, G., Husson, L., Pastier, A. M., Fernández-Blanco, D., Pico,
954 T., Chauveau, D., ... & Pedoja, K. (2022). High interstadial sea levels

- 955 over the past 420ka from the Huon Peninsula, Papua New Guinea.
956 Communications Earth & Environment, 3(1), 256.
957
- 958 **24.** de Gelder, G., Solihuddin, T., Utami, D. A., Hendrizan, M.,
959 Rachmayani, R., Chauveau, D., ... & Cahyarini, S. Y. (2023).
960 Geodynamic control on Pleistocene coral reef development: Insights
961 from northwest Sumba Island (Indonesia). Earth Surface Processes
962 and Landforms, 48(13), 2536-2553.
963
- 964 **25.** de Gelder, G., Hedjazian, N., Husson, L., Bodin, T., Pastier, A. M.,
965 Boucharat, Y., ... & Cahyarini, S. Y. (2024). Reconstructing
966 Quaternary sea-level through bayesian inversion of staircase coastal
967 landscapes. <https://doi.org/10.31223/X5B117>
968
- 969 **26.** Dullo, W. C. (2005). Coral growth and reef growth: a brief review.
970 Facies, 51(1-4), 33-48.
971
- 972 **27.** Dumitru, O. A., Dyer, B., Austermann, J., Sandstrom, M. R.,
973 Goldstein, S. L., D'Andrea, W. J., ... & Raymo, M. E. (2023). Last
974 interglacial global mean sea level from high-precision U-series ages
975 of Bahamian fossil coral reefs. Quaternary Science Reviews, 318,
976 108287.
977

- 978 **28.** Dutton, A., & Lambeck, K. (2012). Ice volume and sea level during
979 the last interglacial. *science*, 337(6091), 216-219.
980
- 981 **29.** Dutton, A., & Barlow, N. L. (2019) What do we know about last
982 interglacial sea level?.
983
- 984 **30.** Dutton, A., Villa, A., & Chutcharavan, P. M. (2022). Compilation of
985 Last Interglacial (Marine Isotope Stage 5e) sea-level indicators in the
986 Bahamas, Turks and Caicos, and the east coast of Florida, USA. *Earth
987 System Science Data*, 14(5), 2385-2399.
988
- 989 **31.** Dyer, B., Austermann, J., D'Andrea, W. J., Creel, R. C., Sandstrom,
990 M. R., Cashman, M., ... & Raymo, M. E. (2021). Sea-level trends
991 across The Bahamas constrain peak last interglacial ice melt.
992 *Proceedings of the National Academy of Sciences*, 118(33),
993 e2026839118.
994
- 995 **32.** B. Fox-Kemper, H.T. Hewitt, C. Xiao, G. Aðalgeirsdóttir, S.S.
996 Drijfhout, T. L. Edwards, N.R. Golledge, M. Hemer, R.E. Kopp, G.
997 Krinner, A. Mix, D. Notz, S. Nowicki, I.S. Nurhati, L. Ruiz, J.-B. Sallée,
998 A.B.A. Slangen, Y. Yu, Ocean, cryosphere and sea level change, in
999 *Climate Change 2021: The Physical Science Basis. Contribution of
1000 Working Group I to the Sixth Assessment Report of the
1001 Intergovernmental Panel on Climate Change*, V. Masson-Delmotte, P.

- 1002 Zhai, A. Pirani, S.L. Connors, C. Péan, S. Berger, N. Caud, Y. Chen,
1003 L. Goldfarb, M.I. omis, M. Huang, K. Leitzell, E. Lonnoy, J.B.R.
1004 Matthews, T.K. Maycock, T. Waterfield, O. Yelekçi, R. Yu, B. Zhou,
1005 Eds.(Cambridge Univ. Press, 2021), pp. 1211–1362.
1006
- 1007 **33.** Georgiou, N., Geraga, M., Francis-Allouche, M., Christodoulou, D.,
1008 Stocchi, P., Fakiris, E., et al. (2022). Late Pleistocene submarine
1009 terraces in the Eastern Mediterranean, central Lebanon, Byblos:
1010 Revealing their formation time frame through modeling. *Quaternary*
1011 *International*, 638–639, 180–196.
1012
- 1013 **34.** Georgiou, N., Stocchi, P., Casella, E., & Rovere, A. (2023). Decoding
1014 the interplay between tidal notch geometry and sea-level variability
1015 during the Last Interglacial (Marine Isotopic Stage 5e) high stand.
1016 *Authorea Preprints*.
1017
- 1018 **35.** Hearty, P. J., Hollin, J. T., Neumann, A. C., O’Leary, M. J., &
1019 McCulloch, M. (2007). Global sea-level fluctuations during the Last
1020 Interglaciation (MIS 5e). *Quaternary Science Reviews*, 26(17-18),
1021 2090-2112.
1022
- 1023 **36.** Hibbert, F. D., Rohling, E. J., Dutton, A., Williams, F. H.,
1024 Chutcharavan, P. M., Zhao, C., & Tamisiea, M. E. (2016). Coral

- 1025 indicators of past sea-level change: A global repository of U-series
1026 dated benchmarks. *Quaternary Science Reviews*, 145, 1-56.
- 1027
- 1028 **37.** Horton, B. P., Khan, N. S., Cahill, N., Lee, J. S., Shaw, T. A., Garner,
1029 A. J., ... & Rahmstorf, S. (2020). Estimating global mean sea-level
1030 rise and its uncertainties by 2100 and 2300 from an expert survey.
1031 *NPJ climate and atmospheric science*, 3(1), 18.
- 1032
- 1033 **38.** Husson, L., Pastier, A. M., Pedoja, K., Elliot, M., Paillard, D.,
1034 Authemayou, C., ... & Cahyarini, S. Y. (2018). Reef carbonate
1035 productivity during quaternary sea level oscillations. *Geochemistry,*
1036 *Geophysics, Geosystems*, 19(4), 1148-1164.
- 1037
- 1038 **39.** Janer, D. F. S., Gabuyo, M. R. P., Carrillo, A. D. V., Co, P. E. Y., del
1039 Rosario, A. L. B., Morata, M. J. S., ... & Siringan, F. P. (2023).
1040 Development of Pag-asa Reefs, West Philippine Sea: Role of Relative
1041 Sea Level Change and Wave Exposure. *Philippine Journal of Science*,
1042 152(1).
- 1043
- 1044 **40.** Kennedy, E. V., Roelfsema, C. M., Lyons, M. B., Kovacs, E. M.,
1045 Borrego-Acevedo, R., Roe, M., ... & Tudman, P. (2021). Reef Cover,
1046 a coral reef classification for global habitat mapping from remote
1047 sensing. *Scientific Data*, 8(1), 196.
- 1048

- 1049 **41.** Koelling, M., Webster, J.M., Camoin, G., Iryu, Y., Bard, E. & Seard, C.
1050 (2009) SEALEX-internal reef chronology and virtual drill logs from a
1051 spreadsheet-based reef growth model. *Global and Planetary Change*,
1052 66(1–2), 149–159. Available from: [https://doi.org/10.1016/j.](https://doi.org/10.1016/j.gloplacha.2008.07.011)
1053 [gloplacha.2008.07.011](https://doi.org/10.1016/j.gloplacha.2008.07.011)
1054
- 1055 **42.** Kopp, R. E., Simons, F. J., Mitrovica, J. X., Maloof, A. C., &
1056 Oppenheimer, M. (2009). Probabilistic assessment of sea level during
1057 the last interglacial stage. *Nature*, 462(7275), 863-867.
1058
- 1059 **43.** Liu, J., Milne, G. A., Kopp, R. E., Clark, P. U., & Shennan, I. (2016).
1060 Sea-level constraints on the amplitude and source distribution of
1061 Meltwater Pulse 1A. *Nature Geoscience*, 9(2), 130-134.
1062
- 1063 **44.** Macintyre IG, Burke RB, Stuckenrath R (1977) Thickest recorded
1064 Holocene reef section, Isla Perez core, Alacran Reef, Mexico. *Geology*
1065 5:749–754
1066
- 1067 **45.** Matsumoto, H., Young, A. P., & Carilli, J. E. (2022). Modeling the
1068 relative influence of environmental controls on marine terrace widths.
1069 *Geomorphology*, 396, 107986.
1070
- 1071 **46.** Murray-Wallace, C. V., & Woodroffe, C. D. (2014). Quaternary sea-
1072 level changes: a global perspective. Cambridge University Press.

1073

1074 **47.** O’Leary, M. J., Hearty, P. J., Thompson, W. G., Raymo, M. E.,
1075 Mitrovica, J. X., & Webster, J. M. (2013). Ice sheet collapse following
1076 a prolonged period of stable sea level during the last interglacial.
1077 *Nature Geoscience*, 6(9), 796-800.

1078

1079 **48.** Pastier, A. M., Husson, L., Pedoja, K., Bézoz, A., Authemayou, C.,
1080 Arias-Ruiz, C., & Cahyarini, S. Y. (2019). Genesis and architecture of
1081 sequences of Quaternary coral reef terraces: Insights from numerical
1082 models. *Geochemistry, Geophysics, Geosystems*, 20(8), 4248-4272.

1083

1084 **49.** Pedoja, K., Husson, L., Johnson, M. E., Melnick, D., Witt, C., Pochat,
1085 S., ... & Garestier, F. (2014). Coastal staircase sequences reflecting
1086 sea-level oscillations and tectonic uplift during the Quaternary and
1087 Neogene. *Earth-Science Reviews*, 132, 13-38.

1088

1089 **50.** Pedoja, K., Husson, L., Bézoz, A., Pastier, A. M., Imran, A. M., Arias-
1090 Ruiz, C., ... & Choblet, G. (2018). On the long-lasting sequences of
1091 coral reef terraces from SE Sulawesi (Indonesia): Distribution,
1092 formation, and global significance. *Quaternary Science Reviews*, 188,
1093 37-57.

1094

1095 **51.** Peñalver, L., Pedoja, K., Martin-Izquierdo, D., Authemayou, C.,
1096 Nuñez, A., Chauveau, D., ... & Husson, L. (2021). The Cuban staircase

- 1097 sequences of coral reef and marine terraces: A forgotten masterpiece
1098 of the Caribbean geodynamical puzzle. *Marine Geology*, 440, 106575.
1099 <https://doi.org/10.1016/j.margeo.2021.106575>
1100
- 1101 **52.** Pirazzoli, P. A., Radtke, U., Hantoro, W. S., Jouannic, C., Hoang, C.
1102 T., Causse, C., & Best, M. B. (1991). Quaternary raised coral-reef
1103 terraces on Sumba Island, Indonesia. *Science*, 252(5014), 1834-
1104 1836.
- 1105
- 1106 **53.** Polyak, V. J., Onac, B. P., Fornós, J. J., Hay, C., Asmerom, Y., Dorale,
1107 J. A., ... & Ginés, A. (2018). A highly resolved record of relative sea
1108 level in the western Mediterranean Sea during the last interglacial
1109 period. *Nature geoscience*, 11(11), 860-864.
- 1110
- 1111 **54.** Raftery, A. E., Zimmer, A., Frierson, D. M., Startz, R., & Liu, P.
1112 (2017). Less than 2 C warming by 2100 unlikely. *Nature climate*
1113 *change*, 7(9), 637-641.
- 1114
- 1115 **55.** Rohling, E. J., Grant, K., Bolshaw, M., Roberts, A. P., Siddall, M.,
1116 Hemleben, C., & Kucera, M. (2009). Antarctic temperature and global
1117 sea level closely coupled over the past five glacial cycles. *Nature*
1118 *Geoscience*, 2(7), 500-504.
- 1119

- 1120 **56.** Rohling, E. J., Hibbert, F. D., Grant, K. M., Galaasen, E. V., Irvall, N.,
1121 Kleiven, H. F., ... & Yu, J. (2019). Asynchronous Antarctic and
1122 Greenland ice-volume contributions to the last interglacial sea-level
1123 highstand. *Nature Communications*, 10(1), 5040.
- 1124
- 1125 **57.** Rovere, A., Raymo, M. E., Vacchi, M., Lorscheid, T., Stocchi, P.,
1126 Gomez-Pujol, L., ... & Hearty, P. J. (2016). The analysis of Last
1127 Interglacial (MIS 5e) relative sea-level indicators: Reconstructing
1128 sea-level in a warmer world. *Earth-Science Reviews*, 159, 404-427.
- 1129
- 1130 **58.** Rovere, A., Khanna, P., Bianchi, C. N., Droxler, A. W., Morri, C., &
1131 Naar, D. F. (2018). Submerged reef terraces in the Maldivian
1132 Archipelago (Indian Ocean). *Geomorphology*, 317, 218-232.
- 1133
- 1134 **59.** Rovere, A., Ryan, D. D., Vacchi, M., Dutton, A., Simms, A. R., &
1135 Murray-Wallace, C. V. (2023). The World Atlas of Last Interglacial
1136 Shorelines (version 1.0). *Earth System Science Data*, 15(1), 1-23.
- 1137
- 1138 **60.** Skrivanek, A., Li, J., & Dutton, A. (2018). Relative sea-level change
1139 during the Last Interglacial as recorded in Bahamian fossil reefs.
1140 *Quaternary Science Reviews*, 200, 160-177.
- 1141
- 1142 **61.** Spratt, R. M., & Lisiecki, L. E. (2016). A Late Pleistocene sea level
1143 stack. *Climate of the Past*, 12(4), 1079-1092.

- 1144
- 1145 **62.** Thompson, W. G., & Goldstein, S. L. (2005). Open-system coral ages
1146 reveal persistent suborbital sea-level cycles. *Science*, 308(5720),
1147 401-404.
- 1148
- 1149 **63.** Thompson, W. G., Allen Curran, H., Wilson, M. A., & White, B. (2011).
1150 Sea-level oscillations during the last interglacial highstand recorded
1151 by Bahamas corals. *Nature Geoscience*, 4(10), 684-687.
- 1152
- 1153 **64.** Toomey, M., Ashton, A.D. & Perron, J.T. (2013) Profiles of ocean
1154 island coral reefs controlled by sea-level history and carbonate
1155 accumulation rates. *Geology*, 41(7), 731–734. Available from:
1156 [https://doi.org/ 10.1130/G34109.1](https://doi.org/10.1130/G34109.1)
- 1157
- 1158 **65.** Turcotte, D.L. & Bernthal, M.J. (1984) Synthetic coral-reef terraces
1159 and variations of Quaternary sea level. *Earth and Planetary Science*
1160 *Letters*, 70(1), 121–128. Available from:
1161 [https://doi.org/10.1016/0012- 821X\(84\)90215-2](https://doi.org/10.1016/0012-821X(84)90215-2)
- 1162
- 1163 **66.** Veron, J., Stafford-Smith, M., DeVantier, L., & Turak, E. (2015).
1164 Overview of distribution patterns of zooxanthellate Scleractinia.
1165 *Frontiers in Marine Science*, 1, 81.
- 1166

- 1167 **67.** Vyverberg, K., Dechnik, B., Dutton, A., Webster, J. M., Zwartz, D., &
1168 Portell, R. W. (2018). Episodic reef growth in the granitic Seychelles
1169 during the Last Interglacial: implications for polar ice sheet dynamics.
1170 *Marine Geology*, 399, 170-187.
- 1171
- 1172 **68.** Waelbroeck, C., Labeyrie, L., Michel, E., Duplessy, J. C., Mcmanus, J.
1173 F., Lambeck, K., ... & Labracherie, M. (2002). Sea-level and deep
1174 water temperature changes derived from benthic foraminifera isotopic
1175 records. *Quaternary science reviews*, 21(1-3), 295-305.
- 1176
- 1177 **69.** Webster, J.M., Wallace, L.M., Clague, D.A. & Braga, J.C. (2007)
1178 Numerical modeling of the growth and drowning of Hawaiian coral
1179 reefs during the last two glacial cycles (0-250 kyr). *Geochemistry,*
1180 *Geophysics, Geosystems*, 8(3), n/a. Available from:
1181 <https://doi.org/10.1029/2006GC001415>
- 1182
- 1183 **70.** Whitney, B. B., & Hengesh, J. V. (2015). Geomorphological evidence
1184 for late Quaternary tectonic deformation of the Cape Region, coastal
1185 west central Australia. *Geomorphology*, 241, 160-174.